

ISOCAM-CVF 5-12 μ m spectroscopy of Ultraluminous Infrared Galaxies ¹Q.D. Tran¹, D. Lutz¹, R. Genzel¹, D. Rigopoulou¹, H.W.W. Spoon², E. Sturm¹, M. Gerin³, D.C. Hines⁴, A.F.M. Moorwood², D.B. Sanders⁵, N. Scoville⁶, Y. Taniguchi⁷, M. Ward⁸

dantran@mpe.mpg.de

ABSTRACT

We present low resolution mid infrared spectra of 16 ultraluminous infrared galaxies (ULIRGs) obtained with the CVF spectroscopy mode of ISOCAM on board the Infrared Space Observatory ISO. Our sample completes previous ISO spectroscopy of ultra- and hyperluminous infrared galaxies towards higher luminosities. The combined samples cover an infrared luminosity range of $\sim 10^{12-13.1} L_{\odot}$.

To discriminate AGN and starburst activity, we use the AGN-related mid-infrared continuum and the starburst-related 6.2, 7.7, 8.6, 11.3 μ m mid infrared emission bands attributed to aromatic carbonaceous material. For about half of the high luminosity ULIRGs studied here, strong aromatic emission bands suggest starburst dominance. Other spectra are dominated by a strong AGN-related continuum with weak superposed emission features of uncertain nature. Our sample contains one unusual example, IRAS F00183-7111, of an AGN that is highly obscured even in the mid-infrared.

An improved method to quantitatively characterize the relative contribution of star formation and AGN activity to the mid-infrared emission of ULIRGs is presented. The ULIRG spectra are fitted by a superposition of a starburst and an AGN spectrum, both of which may be obscured at different levels. Models in which starburst and AGN obscuration differ are significantly more successful than models with a single extinction. Previous results based on a simpler line-to-continuum measure of aromatic emission

¹Max-Planck-Institut für extraterrestrische Physik, Postfach 1603, 85740 Garching, Germany

²European Southern Observatory, Karl-Schwarzschild-Straße 2, 85748 Garching, Germany

³Ecole Normale Supérieure - Radioastronomie, 24 Rue Lhomond, F-75231 Paris, France

⁴Steward Observatory, The University of Arizona 933 N. Cherry Ave., Tucson, AZ 85721, USA

⁵Institute for Astronomy, University of Hawaii, 2680 Woodlawn Drive, Honolulu, HI 96822, USA

⁶California Institute of Technology, Pasadena, CA 91125, USA

⁷Astronomical Institute, Tohoku University, Aramaki, Aoba, Sendai 980-8758, Japan

⁸Department of Physics and Astronomy, Leicester University, Leicester, LE1 7RH, UK

strength are confirmed, further supporting the robustness of the aromatic emission feature as a diagnostic of ULIRG power sources.

As dominant source of the bolometric luminosity, starbursts prevail at the lower end and AGNs at the higher end of this range. The transition between mostly starburst and mostly AGN powered occurs at $\sim 10^{12.4}$ to $10^{12.5} L_{\odot}$, and individual luminous starbursts are found up to $\sim 10^{12.65} L_{\odot}$.

Subject headings: infrared: galaxies, galaxies: starburst, galaxies: active

1. Introduction

Recently, mid infrared spectroscopy has been used increasingly as a tool for studies of ultra-luminous infrared galaxies (ULIRGs, $L_{\text{IR}} > 10^{12} L_{\odot}$, see Sanders & Mirabel (1996) for a review). The presence of starbursts and active galactic nuclei (AGN) in ULIRGs (and coexistence in some of them) has been known for quite some time, but the question which of the two dominates the luminosity has been difficult to answer because of the large columns of obscuring dust found towards the nuclear regions of these gas- and dust-rich systems. High sensitivity and complete coverage of the infrared spectrum by ESA’s Infrared Space Observatory (ISO, Kessler et al. 1996) have considerably advanced the use of infrared spectroscopy to penetrate this obscuring dust, and to probe for the sources of the huge luminosity of ULIRGs.

Fine structure line and aromatic emission feature observations with ISO-SWS and ISOPHOT-S of a sample of 15 bright ULIRGs suggest that most ULIRGs are predominantly starburst-powered (Genzel et al. 1998). The PAH method has been extended to a larger sample (Lutz et al. 1998; Rigopoulou et al. 1999), allowing to probe for evolutionary effects expected in a scenario where starburst activity gives way to a quasar-like AGN buried inside the ULIRG (Sanders et al. 1988). Comparison of optical and mid-infrared spectroscopic diagnostics (Lutz et al. 1999; Taniguchi et al. 1999) demonstrated surprisingly good agreement if optical LINERs are interpreted as starbursts. This finding also suggests that AGN in ULIRGs usually make their presence known optically at least in certain directions, instead of being fully embedded by large obscuring columns of dust.

This paper presents the result of a solicited program in ISO open time, which addresses two main issues only partly covered by previous work. First, and most important, at which luminosity does the transition from ‘predominantly starburst-powered’ to ‘predominantly AGN-powered’ occur? On one hand, the ISO observations of Genzel et al. (1998) and Lutz et al. (1998) suggest that not only luminous infrared galaxies with $L_{\text{IR}} < 10^{12} L_{\odot}$, but also most ULIRGs above this threshold

¹Based on observations with ISO, an ESA project with instruments funded by ESA Member States (especially the PI countries: France, Germany, the Netherlands and the United Kingdom) with the participation of ISAS and NASA

are predominantly starburst powered. On the other hand, optical and mid-infrared observations of hyperluminous infrared galaxies (Hines et al. 1995; Hines et al. 1999; Taniguchi et al. 1997; Aussel et al. 1998) support a previous consensus that AGN dominate these hyperluminous systems (but note the intriguing possibility that far-infrared peaks in some luminous AGN may trace even higher star formation related luminosities, e.g. Haas et al. 1998). The luminosity at which *local* ULIRGs ($z < 0.4$) – on average – switch from starburst to AGN dominated is a quantity with implications for various fields ranging from the interpretation of sources found in recent submm surveys (Hughes et al. 1998; Barger et al. 1998) to explanation of the hard X-ray background (Comastri et al. 1995). Simple arguments based on the free fall time of the gas mass concentrated in the inner region of ULIRGs and the nucleosynthesis efficiency suggest a maximum luminosity of a starburst event approaching $10^{13} L_{\odot}$ (Heckman 1994), the limit depending on gas mass, spatial scale, and initial mass function properties. Observational evidence is clearly needed. Despite its size of ~ 60 sources, the ULIRG sample presented by Lutz et al. (1998) and Rigopoulou et al. (1999) is not optimal for this task: It is selected basically as flux limited at $60\mu\text{m}$ and dominated by low to moderate luminosity ULIRGs, because of the steep ULIRG luminosity function (Sanders & Mirabel 1996). The preliminary analysis of Lutz et al. (1998) in the mid-infrared and a recent study of Veilleux et al. (1999) in the optical/NIR infrared showed that the presence of AGN in ULIRGs increases with the luminosity of the object. However, these studies clearly call for improved statistics above $\sim 10^{12.3} L_{\odot}$ in order to better determine the transition to AGN-dominated systems.

The second issue addressed by this paper is related to the use of PAH features as an AGN/starburst diagnostic. Mid-infrared spectra of most galaxies show the 6.2, 7.7, 8.6, and $11.3\mu\text{m}$ features attributed to aromatic carbonaceous material (Duley & Williams 1981; Léger & Puget 1984; Sakata et al. 1987; Papoular et al. 1989). Among several popular designations for these bands will be designated hereafter by the terms PAH (polycyclic aromatic hydrocarbon) or UIB (unidentified infrared bands, because of remaining uncertainties on the precise nature of the aromatic carrier). Groundbased observations of these features and a companion at $3.3\mu\text{m}$ first demonstrated that their equivalent width is larger in starburst galaxies than in classical AGNs (Moorwood 1986; Roche et al. 1991). ISO spectroscopy has further strengthened this link by demonstrating the anti-correlation between feature strength relative to the continuum and the ionization state of the gas (Genzel et al. 1998). Spatially resolved ISOCAM-CVF observations of nearby AGN support this interpretation by showing the PAH features contrast to be weak near the central AGN but strong in the circumnuclear region likely dominated by star formation (e.g. Cen A, NGC 1068: (Laurent et al. 1999), Circinus: (Moorwood 1999)). Despite this solid empirical basis, special care is required in analyzing PAH spectra of ULIRGs for AGN or starburst dominance. All components of the spectrum – continuum and emission features, AGN or starburst – may be unusually obscured, and the limited wavelength coverage of ISOPHOT-SL spectra ($5.8\text{--}11.6\mu\text{m}$ observed wavelength) makes continuum definition difficult. Here, the extended wavelength range of ISOCAM-CVF ($5\text{--}16.5\mu\text{m}$) is beneficial in reaching the long wavelength side of the broad $9.7\mu\text{m}$ silicate absorption feature.

Our paper is organized as follows: We discuss sample selection, observations and data analysis

in Section 2. Section 3 presents the observational results. Section 4 establishes a new quantitative method to determine the contribution of starburst and AGN activity to the mid-infrared spectra, and compares it with the method used by Genzel et al. (1998), Lutz et al. (1998) and Rigopoulou et al. (1999). In Section 5, we discuss the properties of ULIRGs as a function of luminosity, combining our sample with the results of the ISOPHOT-S sample and with ISOCAM results on HYLIRGs. Finally, we conclude in section 6.

2. Observations and data reduction

2.1. Sample and observing strategy

The solicited observing program presented here was defined in the last third of the ISO mission when it had become apparent that low resolution spectroscopy of ULIRGs was a promising tool, and that studies of ULIRGs needed to be extended towards higher luminosities. The sample selection is strongly driven by the visibility constraints of the ISO satellite during the final six months of the mission. ULIRGs were selected from the samples of Fisher et al. (1995), Kim (1995), Clements et al. (1996), and the QDOT sample (Lawrence et al. 1999). Six sources were chosen from these catalogues with $L_{\text{IR}} > 10^{12.5} L_{\odot}$ that had reasonable ISO visibility during the remaining mission, plus an additional ten slightly lower luminosity sources that could be accommodated within the available observing time. Table 1 lists basic properties of the sample galaxies. Throughout this paper, we follow the convention reported by Sanders & Mirabel (1996) to compute the 8-1000 μm luminosity L_{IR} , adopting $H_0=75 \text{ km s}^{-1} \text{ Mpc}^{-1}$ and $q_0=0.5$, and IRAS FSC fluxes (IRAS 03521+0028, IRAS 18030+0705: PSC). Most of our sources are lacking detections in some of the IRAS photometric bands. In those cases, we replaced the missing fluxes by estimates based on the 60 μm fluxes and average colors of the Sanders et al. (1988) ULIRGs. The observations included the source IRAS 03452+2320 taken from the sample of Fisher et al. (1995), which is not listed in Table 1. We did not detect a signal at its position. We believe this reflects an infrared cirrus related misidentification in the Fisher et al. (1995) sample rather than mid-infrared faintness of a true ULIRG, since Crawford et al. (1996) failed to detect the same source in radio continuum.

Our sample is certainly heterogeneous : it was selected from ULIRG surveys of different limiting 60 μm flux, with a preference for high luminosity targets but not implementing a strict lower cutoff, and strongly driven by ISO visibilities. None of the selection criteria, however, should significantly bias our sample in mid-IR spectral properties or AGN content. In particular, no AGN-related IRAS color criteria like the 25/60 μm flux ratio were applied (de Grijp et al. 1985; Sanders et al. 1988a). A slight tendency towards favoring AGN at higher redshifts/luminosities is induced by the 60 μm selection which is effectively at $\sim 45\mu\text{m}$ rest wavelength for the most distant targets. We have not attempted to correct for this since detailed far-infrared spectral energy distributions are unavailable for these faint IRAS sources, and since the effect will be negligible for our small and still fairly local sample. The sample is hence suited to study the AGN content of ULIRGs, bridging the gap between

the lower luminosity ULIRGs studied with ISOPHOT-S (Lutz et al. 1998; Rigopoulou et al. 1999) and the two HyperLuminous Infrared Galaxies (HYLIRGs) observed by ISO (Taniguchi et al. 1997; Aussel et al. 1998). Figure 1 shows the distribution of infrared luminosities both for our sample and the combined ISO database.

The observations presented here used the Circular Variable Filter (CVF) mode of the ISOCAM camera (Cesarsky et al. 1996) rather than the ISOPHOT-S mode with which most other low resolution ULIRG spectra were obtained and which is efficient in building a large sample of relatively bright sources. The ultimate sensitivity achieved in a long CVF integration time is better, and the need for stabilization overheads was no major concern for our moderate number of very faint sources. In addition, the extended long wavelength coverage is crucial in targeting objects up to $z \sim 0.4$, and in probing an extended rest wavelength range. Since our sources are expected to be spatially unresolved, we have chosen the most sensitive setting with $6''$ pixels and a total FOV of about $3'$. The observed wavelength range varies from source to source, the short end being defined by $5\mu\text{m}$ rest wavelength and the long end either by $12\mu\text{m}$ rest wavelength or, for high redshift sources, by $16\mu\text{m}$ observed wavelength where the sensitivity of CVF observations starts to decrease quickly. In order to increase redundancy and to enable correction of the transients of the ISOCAM detector, each CVF scan has been done in up and down direction. To reconcile the need for detector stabilization (10 frames of 5sec exposure at each wavelength) with the total number of wavelength steps and practical limits on observing time, we have executed up- and down-scans with interleaved wavelength steps. The total observing time per source including overheads was typically 2.5 hours. Each final spectrum is composed by about 120 wavelength steps and has an average resolution of $R \approx 35$.

2.2. Data reduction

Reductions have been carried out with the Cam Interactive Analysis (CIA) software¹⁰. The dark current has been estimated with the dark model described by Biviano & Sauvage (1999). This gives better results than using the two offset observations we have taken before and after the CVF observation. We used the multi-median resolution deglitching method (Starck et al. 1999) to remove glitches, and then additionally deglitched manually a square of 3 by 3 pixels centered on the source. To correct the transient effect of the detector the inversion method developed at IAS (Coulais & Abergel 1999) was used. The calibration of the flux was performed using the standard spectral response function of CIA.

Appendix A presents a reduction scheme which allows to quantify the spectrum of a target, with its S/N ratio and the systematic error introduced by the reduction method (the total uncertainty

¹⁰CIA is a joint development by ESA Astrophysics division and the ISOCAM consortium led by the ISOCAM PI, C. Cesarsky, Direction des Sciences de la Matière, CEA, France.

on the flux is about 5 mJy). It also allows us to determine the position of the fairly faint source with sub-pixel accuracy. The typical uncertainty of the position is $5''$, including S/N and ISO pointing uncertainty.

One target (IRAS 00406-3127) of the set had not been acquired by ISOCAM because of a telemetry drop. For IRAS F02115+0226 there was no source detection. The S/N ratio observed for IRAS F02455-2220 is not high enough to reliably determine the PSF correction described in the Appendix. However, the observed spectrum can be taken as a lower limit, using only the signal from the brightest pixel. For the remaining 13 targets, the data reduction has been applied successfully.

3. Results

The rest-frame spectra for the 13 sources are shown in Figure 2. The shaded confidence area around the spectrum represents the RMS plus the systematic error. Table 1 lists the position of the sources as obtained by the PSF fitting method (see Appendix), and the IRAS fluxes. All targets were found to be point like sources at ISOCAM resolution. One target has been found to be significantly offset from the IRAS PSC position: IRAS 18030+0705. The offset is about one arcminute. We checked the original IRAS data using XSCANPI and found a source with fluxes similar to those listed in the PSC, but centered on the ISOCAM position. The origin of this position discrepancy is unknown. The FSC fluxes were adopted for the ULIRGs detected by ISOCAM except for IRAS 18030+0705 and IRAS 03521+0028 for which we used PSC fluxes.

From previous studies, the following components are expected to be present in ULIRG spectra, but not necessarily together in *one* spectrum :

- UIB emission features at 6.2, 7.7, 8.6 and 11.3 microns, mainly originating from star forming regions of the galaxies. This UIB emission can be also coupled with a continuum of hot dust present in the most energetic H II regions of the starburst.
- An AGN continuum from the hot dust present in the vicinity of the AGN, e.g. in a dust torus or at larger scale in the narrow line region.
- Strong absorption, both continuous and in features like the silicate $9.7 \mu\text{m}$ one. Absorption may arise either in the surroundings of the AGN or the larger scale ISM. The amount of absorption may be different for AGN and for starburst.

The silicate feature at $9.7\mu\text{m}$ that is usually found in absorption may also mimic emission features. In dust configurations as in some torus models (Pier & Krolik 1992), self-absorbed silicate emission can create an emission peak near $8\mu\text{m}$ that is superficially similar to a faint UIB emission and may be observed in one HYLIRG (Taniguchi et al. 1997). Discrimination of such a ‘fake UIB’ peak and real UIB emission has to rely on the detailed shape of the $8\mu\text{m}$ peak and presence of the other UIB features.

Table 2 summarizes the presence of the UIB bands. About half of the targets exhibit a spectrum with at least the 6.2, 7.7 and 11.3 μm mid infrared bands clearly visible. The remaining targets do not exhibit all these bands, and two none of them significantly. It is striking that almost all the observed ULIRGs show a strong feature at or near 7.7 μm . IRAS F23529-2919 is an exception. Here, the continuum might be so strong that it can dominate the emission of the 7.7 μm emission band. Also, the shape of the 7.7 μm feature is very different in two other galaxies from the typical UIB band. IRAS 22192-3211 and IRAS 00275-2859 have a band which is broader than the one observed in a “normal” starburst galaxy. The signal to noise for IRAS 23515-2917 is lower so it is more difficult to draw a definitive conclusion. A strong continuum has been detected in the two former targets, which supports the presence of an AGN in both sources. The change of the shape of the 7.7 μm feature can be explained in two ways. The carriers of the UIB might be processed in the AGN environment, changing the shape of the spectral emission of these carriers. Such changes in the shape of the 7.7/8.6 μm complex have in fact been observed in some ultra-compact H II regions (Cesarsky et al. 1996a). Alternatively, a “fake” 7.7 μm feature could arise when one observes a high optical depth source with self-absorbed silicate emission. There is no agreement in detail, however, between the broadish 8 μm features in these ULIRGs and the spectral shapes predicted by torus models (Pier & Krolik 1992). A further problem of a ‘torus’ identification of these 8 μm features is that they are not observed in the spectra of template Seyferts and QSOs (Rigopoulou et al. 1999; Clavel et al. 2000).

Another source, IRAS F00183-7111, has a maximum near 8 μm which we do not ascribe to UIBs. Its spectrum is remarkably similar to some deeply obscured objects (d’Hendecourt et al. 1996, NGC 7538 IRS1 : D.Cesarsky unpublished), showing a strong 5-8 μm continuum and an extremely deep silicate absorption. Even an apparent “6.5 μm emission” is indicated in this object which is very likely the result of the absorption of water ice at 6 μm and an absorption feature at 6.85 μm which is of unclear origin (Schutte 1998). The spectrum of IRAS F00183-7111 is thus dominated by a heavily absorbed (AGN) continuum with a possible weak 7.7 μm emission, which might be either due to a classical UIB or self-absorbed silicate emission. In total, it appears to be the only unambiguous example in our data for a type of source considered typical in the classical Sanders et al. (1988) scenario: an extremely obscured AGN.

4. Quantitative diagnostics of the Starburst and AGN activity in ULIRGs

The use of the line-to-continuum ratio of the 7.7 μm band (hereafter L/C) as proposed by Genzel et al. (1998) and Lutz et al. (1998) to distinguish in the *mid-infrared* between starburst-dominated and AGN-dominated ULIRGs is based on evidence that a starburst galaxy presents strong UIB features while AGN presents strong continuum with a low contrast emission features in the nuclear part of the galaxy. This is suggested by ground based observations (Moorwood 1986; Roche et al. 1991), ISO spectroscopy (Genzel et al. 1998; Rigopoulou et al. 1999), and ISO spectro-imaging (Moorwood 1999; Laurent et al. 1999). This also implies that the UIB luminosity of

a galaxy scales with its star formation. Recent studies tend to reinforce this idea : in spiral galaxies, the global $H\alpha$ emission of the disk is correlated with the total MIR emission of UIB (Vigroux et al. 1999; Roussel et al. 2000).

When using these features as tracers of the sources of the total ULIRG luminosity, a further assumption is that the mid-infrared actually probes the active regions and not just a surface layer. This is not trivial since the active regions of ULIRGs are small (Condon et al. 1991; Soifer et al. 2000) and dusty. Depending on dust configuration, a major part of the luminosity could be hidden from mid-infrared view. Genzel et al. (1998) have addressed this problem using the starburst-type mid-infrared nebular spectra of ULIRGs. For ULIRGs, the ratio of the inferred starburst ionizing luminosity to the bolometric luminosity approaches that for template starbursts, indicating that more than half of the luminosity has been traced by the mid-infrared observations. Similar analyses can be made using the luminosity of the PAH features. Rigopoulou et al. (1999) and Genzel & Cesarsky (2000) find that observed PAH luminosities of ULIRGs are well above those of lower luminosity sources, the ratio to bolometric luminosity being only a factor 1.4-2 lower than in starbursts. This factor is plausibly explained by the higher extinction in ULIRGs and perhaps the effect of the more intense radiation field on the PAH emission. We have tentatively repeated this comparison using the extinction correction derived from our fits described below, which however give only fairly uncertain extinction for individual noisy spectra. The mean discrepancy narrows down to a factor 1.2. Thus, the mid-infrared diagnostics are probing the major part of the luminosity.

For a narrow line and emission from a single region, both line and continuum are obscured by the same amount. The width of the PAH feature and the strong wavelength dependence of extinction at the onset of the silicate feature make the PAH L/C less ideal. In some objects the absorption might be so strong that it can mimic a 7.7 band. There are, however, differences in shape and the L/C will normally stay below the cutoff of 1 adopted in previous papers. IRAS F00183-7111 is the only clear example in our sample. Another technical point that has to be verified is the determination of the continuum under the $7.7\mu\text{m}$ feature. In the L/C diagnostic, this continuum is deduced from the linear interpolation of the continuum levels at 5.9 and $10.9\mu\text{m}$, i.e. the L/C ratio is affected by the flux uncertainties at these wavelengths. This is also a systematic source of uncertainty since the $10.9\mu\text{m}$ point is still within the silicate feature and does not probe a clean continuum.

We have explored alternative methods in order to verify the robustness of the L/C ratio with respect to the systematic error induced in the $7.7\mu\text{m}$ continuum determination. First, we constructed the “narrow band” ratio between the flux density at 7.7 and $6\mu\text{m}$. Strong UIB emission will create a high ratio which is not reached by a pure continuum unless it is unrealistically steep over this small wavelength interval. This diagnostic should hence identify strong UIB emission easily but will face problems discriminating weak UIBs from continuum slope variations. The strength of this diagnostic is to avoid any assumption on the shape of the spectrum in the region obscured by the silicate feature. Figure 3 shows the correlation between the L/C and $F(7.7)/F(6)$

diagnostics seen for ULIRGs and template spectra observed by PHOT-S (Rigopoulou et al. 1999), SWS (Sturm et al. 2000), and CAM-CVF (this paper). The dispersion in this plot is explained by the variation in continuum slope and the systematic error of the L/C discussed before. The good correlation of the two diagnostics supports the use of the L/C diagnostic to identify systems that are clearly starburst-like and show strong UIBs. By definition of the F7.7/F6 diagnostic, Figure 3 cannot test the effect of continuum placement uncertainty in the L/C method on measurements of faint residual UIBs in AGN-like systems. The line $F(7.7\mu\text{m})/F(6\mu\text{m})=L/C+1$ is also overplotted in Figure 3 to indicate the asymptotic case where the continuum is flat.

To investigate further how the different spectral components influence the MIR spectrum of a galaxy, we created another diagnostic whose basis is a more physical parameterization of the spectrum.

4.1. Presentation of the model

Our aim is an empirical fitting procedure using the complete mid-infrared low resolution spectra to derive the contribution of the AGN and starburst components to the mid-infrared spectrum. In a second step, results will be extrapolated to the bolometric luminosities. The fit is based on template spectra of dusty starbursts and AGN, and applied to the whole set of ULIRG and template spectra observed by PHOT-S (Rigopoulou et al. 1999), SWS (Sturm et al. 2000), and CAM-CVF (this paper). Since absorption plays an important role for the spectra of dust-rich ULIRGs, we incorporate the effects of absorption that is higher than in the templates. In principle, explaining the mid-infrared spectra of ULIRGs is a problem of three dimensional radiative transfer requiring a consistent treatment of dust, ices, and PAH features. Considerable insight can be gained, however, from a simple superposition of a screen-obscured starburst and a screen-obscured AGN. Arguments in favour of this approach are: (1) The mid-infrared diagnostic reaches most of the active region. Unknown more obscured sources will be minor contributors. (2) The use of an observed AGN template implicitly accounts for warm dust close to the AGN. Screen extinction is a reasonable first approximation for the effect of even more dust around the AGN, since this dust will mostly just absorb in the mid-infrared consider here, and reemit in the far-infrared. (3) An aggregate of star forming regions is in principle better represented by a case where emission and absorption are well mixed. Mixed case extinctions are difficult to determine, however, unless there are probes measured at high S/N over a large range of optical depths, a requirement not met by our spectra. The screen case adopted here will give similar results for optical depths around one, fall short at higher optical depth, but be conservative in the sense of not inferring excessive starburst activity in uncertain cases.

4.1.1. *The Starburst component*

Genzel et al. (1998), Rigopoulou et al. (1999) and Sturm et al. (2000) showed that in the range of the 6-9 μ m UIB bands there is little variation in starburst MIR spectra observed by SWS and PHOT-S. Starburst spectra present some variations at longer wavelength, however. Vigroux *et al.* (1996), noted that in some regions of NGC 4038/4039 the flux at 15 μ m can rise dramatically and dominate the mid infrared spectrum. It can be shown that the MIR spectrum of starburst galaxies is the superposition of two components : one from photodissociation regions (PDR) and one from H II regions (Tran 1998). The PDR component is responsible for the UIB emission and the H II region for the hot dust continuum which becomes important at 12 μ m (Cesarsky et al. 1996a; Verstraete et al. 1996; Roelfsema et al. 1996). This hot dust continuum is probably due to very small grains heated to temperature as high as 200K in some regions. This continuum is very faint at 7 μ m (Cesarsky et al. 1996a; Verstraete et al. 1996; Tran 1998), and is not really noticeable in the spectrum of the majority of starburst galaxies where the PDR contribution (*i.e.* the UIB contribution) dominates in this part of the spectrum (Sturm et al. 2000). For some dwarf metal-deficient starburst galaxies like NGC 5253 and IIZw40 (Rigopoulou et al. 1999, S.Madden private communication), UIBs are nearly absent. In such a case a strong featureless continuum will not be an AGN signature. Since ULIRG are dust rich and not known to be metal-deficient this effect is likely not relevant, and we still consider a strong ULIRG continuum with weak UIBs an AGN signature.

As the (rest)-wavelength range investigated in this paper is between 5 and 12 μ m, the contribution of the hot dust continuum from H II regions will not change drastically the spectrum of the starburst contribution. But one *must* keep in mind that strictly speaking a significant continuum at short wavelengths (5-8 μ m) is not necessarily a tracer of an AGN, but could reveal a higher weight on H II regions in the ISM with respect to photodissociation regions. To break the degeneracy, one has to look at the continuum at 15 μ m since the continuum of an H II region is steeper than the continuum of an AGN (Laurent et al. 1999).

In the present model we assume that the template spectrum of a starburst does not change in a significant way between 5 and 12 μ m (see section 4.2 for the self consistency of this hypothesis). **We have used the M82 SWS spectrum as starburst template spectrum**, supposed to represent the standard line to continuum ratio of the UIB seen in a dusty starburst.

4.1.2. *The continuum component*

Nuclear AGN spectra have low contrast UIB features and mainly present a continuum emitted by hot dust. Obviously, when looking at the total spectrum of a galaxy hosting an AGN, one naturally observes UIB bands from circumnuclear star formation or from the disk of the AGN host (see for instance (Mirabel et al. 1999; Clavel et al. 2000; Moorwood 1999; Alexander et al. 1999)). **The AGN spectrum itself can be described by an intrinsic continuum which can be**

well fitted by a power law¹¹ of variable index (Clavel et al. 2000) subject to absorption by dust especially in the region of the $9.7\mu\text{m}$ silicate absorption feature.

As discussed in the previous subsection, a continuum seen in the mid-infrared may also be due to H II regions. In the wavelength range considered (5-12 μm), there is a degeneracy between the AGN continuum and a continuum coming from an H II region, although an H II continuum is usually steeper and fainter. Our fit invokes a single ‘continuum component’ including both possibilities of an AGN continuum and an unusually strong H II continuum. We will come back to the degeneracy between these two types of continua when discussing fit results.

4.1.3. Dust obscuration

Because ULIRGs are gas and dust rich galaxies (Solomon et al. 1997), the extinction is expected to play a crucial role on shaping the spectrum of these galaxies, even in the mid-infrared (see for instance Arp220, (Sturm et al. 1996)). It is important to test how dust obscuration can affect both UIB dominated and featureless spectra (Rigopoulou et al. 1999). One can argue that mid-infrared ULIRG spectra could be completely dominated by absorption, and that the $7.7\mu\text{m}$ feature, which we identify as an UIB, could result from a deep absorption of a flat continuum (Dudley & Wynn-Williams 1997). This could be the case in the strongly absorbed galaxy F00183-7111. We want to test more generally whether it is possible to produce an emission feature around $8\mu\text{m}$ by a power law continuum affected by an absorption law or whether a simple UIB spectrum affected by absorption is preferred.

We used two absorption laws, the ‘classical’ Draine and Lee (1984) absorption law and one composite absorption law derived from the Galactic Center-SgrA* spectrum (hereafter GC or GC-SgrA*). The GC extinction law has a higher extinction level between 3 and $7\mu\text{m}$ (Lutz et al. 1996; Lutz 1999a). Since this law is derived from hydrogen recombination lines and does not sample the silicate feature well, we have supplemented it with points deduced from the GC continuum spectrum itself. They have been computed assuming that the intrinsic GC spectrum is a power law spectrum absorbed by a dust screen. The extinction law and the exponent of the power law have been adjusted in order to fit the extinction deduced from the hydrogen lines and the GC spectrum itself. This procedure is adequate since we cover only a limited wavelength range, and since the dust in front of the Galactic center is close to the ideal screen case. This absorption law has two main peculiarities: a flatter absorption between 3 and $7\mu\text{m}$, and a narrower silicate feature than what the Draine and Lee curve predicts (see Figure 4).

These two absorption laws have been used to represent variations in dust properties as possible in extreme environments such as close to an AGN. Comparison of the M82 and NGC 1068 SWS spectra (Sturm et al. 2000) suggests such variations at least for absorption *features*. Because of the

¹¹The ‘power law’ does not mean non-thermal emission, and thus it is a parameterization of the dust continuum.

possibility of such variations, absolute A_V values derived from the model are somewhat uncertain. The main emphasis is to test whether the shape of the ULIRG spectra can be reproduced well.

4.1.4. *The different models*

The two spectral components and obscuration have been used to construct four types of models in two classes:

- The first class is based on the assumption that the starburst component and the continuum component are obscured by the same dust screen. Models of this class vary in extinction properties: the dust extinction law is either a “pure” Draine and Lee law, or a “pure” GC extinction law or a mixture of the two.
- The second class allows different obscuration of the two components and is clearly more realistic. The two different contributions (continuum and starburst) are not necessarily located in the same physical region and therefore do not suffer the same extinction.

Table 3 provides the formal description of the different models used. Models 1a, 1b and 2 refer to the first class, while models 3a-d and 4 refer to the second class. In two cases (2 and 4), the extinction law is a linear combination of the GC extinction law and the Draine and Lee one. This combination is not constrained by observations but included in our modeling as a comparison to other models with different degrees of freedom.

4.2. Testing the validity of the model

To validate the model, the fit quality is quantified first. Second, the results from test fits to template starburst and AGN spectra are investigated, and compared to observations of “mixed” sources where the AGN and starburst relative contributions are well known from spatially resolved data.

4.2.1. *Quality of model fits*

Figure 5 shows some examples of fits to ULIRG spectra using model 3a. The figure includes AGN and starburst-like spectra of both high and low S/N. Fits using other models tend to be slightly worse but still acceptable. The first conclusion is that the models presented in Table 3 can give a reasonable fit for all ULIRG spectra. This implies that the assumptions of these models (*e.g.* a MIR spectrum of a ULIRG is a superposition of a continuum component and a starburst component extinguished by a dust-rich ISM) are not in obvious contradiction with observations.

To better quantify the quality of the various models we adopt the indicator $\frac{\chi^2}{N_{\text{free}}} = \frac{\sum (F_{\lambda}^{\text{obs}} - F_{\lambda}^{\text{mod}})^2}{\sum (\sigma^{\text{obs}})^2} \frac{1}{N_{\text{free}}}$ where F_{λ}^{obs} is the observed flux density, F_{λ}^{mod} is the model flux density, σ^{obs} is the rms of the observed flux density. The summation is done over *all* ULIRG spectra, and N_{free} is the sum of degrees of freedom of modeled spectra. With this indicator the quality of the different models can be compared: the closer to 1., the better. Table 3 presents the mean $\frac{\chi^2}{N_{\text{free}}}$ both for our complete ULIRG sample, and for a high quality subset with observed S/N greater than 3.

4.2.2. Comparison with template sources.

We have obtained model fits for various starburst, AGN, and mixed template sources. A first result can be obtained from a comparison of the two classes of models for the mixed templates Circinus and Centaurus A. Figure 6 shows the obvious superiority of models where the extinction towards the AGN is different from that towards the starburst. Fully equivalent good fits are achieved for models 3a-3c.

Figures 7 and 8 show the observed spectrum and the fitted spectrum computed with model 3a, for several starburst and AGN templates. The Galactic center has been grouped with the AGNs since the very center shown here is also a continuum source devoid of UIBs (Lutz et al. 1996). The absence of these features in the GC-SgrA* spectrum is due to the presence of an H II-region with an intense radiation field that probably destroys the UIB carriers. We overlay the contributions of the starburst component and the contributions of the continuum component. As expected, the starburst component dominates totally the modelled spectrum for the starburst galaxies. Similarly, a quasi-pure continuum contribution is needed to fit the AGN spectra, with extinction being negligible in many cases but significant in others (NGC 5506). The low metallicity galaxy NGC 5253 (not shown) is well fitted by a strong continuum contribution and weak UIBs. The fits to the starburst templates (Fig. 7) show at their long wavelength end a varying contribution of a faint steeply rising continuum. Most likely, this is due to variations in the strength of the $15\mu\text{m}$ VSG (Very Small Grains) continuum, a conclusion also reached by Sturm et al. (2000) on the basis of the SWS spectra of M82 and NGC 253.

A further test is to apply the model to objects which are well known to be composite, containing both starburst and an AGN. In Figure 9 spectra of four such objects are presented, showing plausible decompositions into the starburst and continuum components. A stringent test can be obtained for Centaurus A and Circinus which have both been observed by ISOCAM/CVF at high spatial resolution (Mirabel et al. 1999; Moorwood et al. 1999 and in preparation). These observations allow us to separate the contribution of the nucleus and the surrounding star-forming regions, and thus a direct test of our model decomposition. The spectrum of the Centaurus A nucleus, extracted from the ISOCAM-CVF observation, is overplotted in Figure 9. The modelled continuum contribution is indeed very similar to the observed spectrum of the nucleus, confirming the validity of our approach. We performed the same comparison for the Circinus galaxy (A.F.M. Moorwood,

private communication) and find the same good agreement between the observed nuclear continuum and the modelled continuum contribution. At least for these two sources, the separation into two contributions (continuum and starburst) is reliable.

4.3. Results of the modelling of starburst and continuum contributions

Table 3 shows that the two classes of models do not reproduce the ULIRG spectra equally well. It is obvious that the models of the second class, where extinctions of continuum and starburst are different, are in better agreement with the observations. This better accuracy is not explained trivially by the increasing number of free parameters. Model 2 which has the same number of free parameters as the ‘good’ models 3a-c is clearly less successful. That means, more flexibility in the shape of the extinction does not improve the fit significantly, while invoking different extinction towards the starburst and AGN does. This lends support to the plausible idea that two different extinctions are applicable to the physically distinct starburst and AGN parts of a ULIRG. Comparing the continuum and starburst extinction derived by our fit procedure, we find the continuum extinction to be slightly smaller on average. This is plausible if the obscuring dust is not distributed with spherical symmetry. We note, however, that this result should be considered tentative given the considerable uncertainty of individual A_v values.

Figure 10 compares the L/C ratio used in previous papers with the ratio of the integrated 5-10 μ m fluxes contained in the continuum contribution and in the starburst contribution as deduced from the model 3a. In this plot we also add the starburst and AGN comparison samples as described by Rigopoulou et al. (1999). The two indicators are well (anti)correlated. This correlation shows *a posteriori* the consistency of the two indicators. Table 4 displays the individual value of L/C and the ratio of the integrated 5-10 μ m fluxes contained in the continuum contribution and in the starburst contribution.

Genzel et al. (1998) and subsequent papers adopted a L/C threshold of 1 to discriminate between starburst and AGN dominated systems. At this threshold, the flux ratio of the continuum and starburst components, each integrated over the 5-10 μ m range, will be larger than one, simply because the UIBs are relatively narrow features. This is reflected in Figure 10. The purpose of the threshold, however, is to identify the component dominating the bolometric luminosity and not just the 5-10 μ m flux. The mid-infrared contributions have to be extrapolated to the bolometric contributions. Using the spectral energy distributions of M82 and of the central region of NGC 1068 as starburst and AGN templates (Sturm et al. 2000 for M82, including IRAS points and correcting for aperture effects), we find the ratio $L_{5-10\mu m}/L_{IR}$ about 2.5 times greater in the case of the AGN than for starbursts. Very similar values are obtained for other AGN templates (NGC 4151, 3C273), consistent with the notion of stronger mid-IR continua in Seyferts than in starbursts (de Grijp et al. 1985). Orientation related variations in mid-infrared Seyfert continua (Clavel et al. 2000) caution that there will be some scatter in these bolometric corrections for individual AGN. In the remainder of this paper, we will apply the factor of 2.5 wherever total

infrared (i.e. bolometric) quantities are discussed. Taking into account the correction factor 2.5, Figure 10 confirms the L/C threshold of 1 as a sensible one for differentiating between sources dominated by the starburst component and those dominated by the AGN component.

5. Discussion

5.1. Mid-infrared spectra and power sources of the highest luminosity ULIRGs

Determination of the power source of the highest luminosity ULIRGs is a prime goal of our project, extending the ISOPHOT-S sample which is dominated by lower luminosity sources (Lutz et al. 1998; Rigopoulou et al. 1999). Figure 11 displays the L/C ratio for the CAM-CVF ULIRGs together with data from Lutz et al. (1998) and the two hyperluminous sources observed by ISO (Taniguchi et al. 1997; Aussel et al. 1998). The UIB L/C is used to classify sources as starburst-like if $L/C > 1$ or AGN-like if $L/C < 1$. From our enlarged database, we confirm that most ULIRGs are starburst dominated in the mid-infrared but that there is a trend towards AGN-like ULIRGs at higher luminosities. In our sample which contains 17 sources above $L_{\text{IR}} = 10^{12.4} L_{\odot}$, the highest luminosity source classified as starburst is at $10^{12.65} L_{\odot}$ (IRAS 03835-6432). Such a luminosity limit for the ‘most luminous starburst’ is in agreement with the timescale argument given by Heckman (1994). Adopting the bolometric luminosities of our sources and sizes like those derived by Soifer et al. (2000) for the mid-IR emitting region of ULIRGs, the surface brightness will exceed the limit for starbursts suggested by Meurer et al. (1997). Individual star forming region are known to exceed this limit, however, and the huge gas concentration in the centers ULIRGs provides sufficient fuel. Additionally, Meurer et al. (1997) derived their limit using, for similar sources, $H\alpha$ -based sizes which are larger than the mid-IR ones found by Soifer et al. (2000), thus staying below the actual surface brightness. Even in our sample enriched in luminous ULIRGs, statistics at the highest luminosities is limited, thus maintaining the possibility for higher luminosity starbursts. Given the modest sample size, it is difficult to assign an accurate value for the luminosity at which half of the sources are starburst and half AGN dominated. From Figure 11, this occurs most likely at luminosities $10^{12.4} L_{\odot}$ to $10^{12.5} L_{\odot}$.

The trend from starburst dominance for most ‘normal’ ULIRGs to AGN dominance at the highest luminosities now consistently emerges from a variety of indicators: Mid-infrared continuum (Sanders et al. 1988a), mid-infrared spectroscopy (Lutz et al. 1998 and this paper), and optical spectroscopy (Veilleux et al. 1999). As noted by (Lutz et al. 1999), the good agreement between optical and mid-infrared suggests that AGN in ULIRGs do not remain fully embedded for long but manage to break the obscuring screen at least in certain directions.

The highest luminosity ‘starburst-like’ systems appear well above our cutoff L/C of 1, but below the $L/C \sim 3$ typical for starbursts and lower luminosity ULIRGs. This can be interpreted in different ways. Either they contain a noticeable though not dominant AGN component, or the increased continuum contribution is due to an increase in the H II-region related continuum, as

might be reasonable for sources with very high star formation rates in a small region.

5.2. The nature of the mid-infrared continuum

The simple L/C method will not be able to break the degeneracy for the origin of ULIRG mid-infrared continua. Also, the parameterization chosen for our fits (Sect. 4.1) describes the spectrum of a ULIRG in terms of just two components : a UIB-dominated starburst component and a continuum component which is either due to an AGN or extra H II region contributions. If the relative weight of ‘PDR-like’ and ‘H II region-like’ components varies for different starburst conditions, as seen e.g. for different regions of the Antennae galaxies (Vigroux et al. 1996), assigning the continuum entirely to an AGN may be misleading. The nature of the continuum has to be investigated in more detail to quantify the fraction of energy radiated by the AGN (AGN continuum) and by star formation activity (UIB-dominated component plus H II region continuum).

It is possible to break the continuum degeneracy by using the slope of the continuum (Laurent *et al.* 1999). The ratio of the fluxes at $6\mu\text{m}$ and $15\mu\text{m}$ is different for an H II region and a continuum emitted by the dust (torus) surrounding an AGN. Dust in the inner parts of H II regions emits a mid-infrared spectrum that is steep over our wavelength range. This can be seen both in Galactic H II regions (Verstraete et al. 1996; Cesarsky et al. 1996) and in extragalactic regions of particularly concentrated star formation, e.g. the star forming knot A in the Antennae galaxies (Vigroux et al. 1996; Mirabel et al. 1998). In contrast, the continuum emitted by hot AGN dust is much flatter in the mid-infrared, as shown by the examples of Cen A (Mirabel et al. 1999) and NGC1068 (Lutz et al. 2000).

Because of the presence of the UIB emission and silicate absorption features, the steepness of the continuum can be determined reliably only with sufficient wavelength coverage, ideally from $6\mu\text{m}$ or less to $15\mu\text{m}$ (rest wavelength). This condition is not met by the ISOPHOT-S spectra which form most of the ISO database of low resolution ULIRG spectra but cut at less than $11\mu\text{m}$ rest wavelength for most ULIRGs. It is partially met for the ISOCAM-CVF spectra presented in this paper which typically extend to rest wavelength about $12\mu\text{m}$. It is instructive to discuss the case of Arp 220 for which a full CVF spectrum is available (Charmandaris et al. 1997). Arp 220 shows 6.2 and $7.7\mu\text{m}$ UIBs on no or weak continuum, whereas the continuum in the 11 - $15\mu\text{m}$ region is clearly stronger than in a standard M82-type starburst spectrum. This suggests a strong but steep H II continuum as in the star forming knot A of the Antennae, subject to even higher extinction (see Figure 12).

The case is less clear for our spectra which do not extend to $15\mu\text{m}$. Some spectra suggest a strong but steep continuum at the long wavelength end of a UIB dominated spectrum (e.g. IRAS 03521+0028) while others are fit by a UIB dominated spectrum plus a flat continuum (e.g. IRAS 18030+0705). At the limited wavelength coverage, the uncertainties are considerable, also taking into account that fits are affected by some 7 - $8\mu\text{m}$ features not showing the typical PAH shape (Sect.

3).

5.3. Model results: Contributions of starburst and AGN activity

Our model can be used to better quantify the contribution of starburst and AGN activity independent from the L/C criterion used earlier. We measured the mid infrared fluxes emitted by starburst and continuum contribution (not dereddened) integrated over the wavelength range 5-10 μ m (similar to the filter LW2 of ISOCAM). When discussing total infrared (bolometric) contributions instead of 5-10 μ m ones, the different AGN and starburst SEDs are considered by increasing the starburst contribution by the correction factor 2.5 derived in Sect. 4.3. Since we were not able to reliably break the degeneracy of AGN and H II region continuum for our wavelength coverage and signal-to-noise ratio, we explored two extreme cases for the origin of the continuum, reality most likely being in between.

The first scenario assumes that the continuum is coming entirely from an AGN. The examples of H II region continua discussed above, however, clearly argue for *some* star formation contribution to the continuum. It is unlikely that an almost pure continuum spectrum is produced in this way. The only star-formation powered galaxies approaching this case are low metallicity dwarfs like NGC 5253, an unlikely match to the ULIRG situation. We hence have adopted the following second extreme scenario: All faint continua, defined as emitting less than 50% of the total 5-10 μ m flux, are assumed to be due to star formation, while all stronger ones are due to an AGN.

Figure 13 shows the median ratio of the energy emitted by the starburst component to the total energy emitted ($F_{5-10\mu\text{m}}(\text{Starburst})/F_{5-10\mu\text{m}}(\text{Total})$) of ULIRGs presented in Table 4 and two HYLIRGs (Taniguchi et al. 1997; Aussel et al. 1998), versus the total infrared luminosity. A trend towards AGN dominance at high luminosity is again clearly seen. The cutoff between starburst-dominated galaxies and AGN-dominated galaxies lies at $L \approx 10^{12.4-12.5} L_{\odot}$. The significance of this trend can be tested by dividing the luminosity range into the bins $L_{\text{FIR}} = 10^{11.8-12.4} L_{\odot}$ and $L_{\text{FIR}} = 10^{12.4-13.0} L_{\odot}$ and using respectively the Kolmogorov-Smirnov's test and the Student's t-test to test if the two samples follow the same distribution or have the mean value. The probability for such hypotheses are 1.0×10^{-4} (resp. 1.3×10^{-4}), demonstrating that the trend is statistically very significant. We also perform the two statistical test while removing the two most luminous galaxies ($L_{\text{FIR}} > 10^{13} L_{\odot}$). Probabilities are then 9.0×10^{-4} and 5.0×10^{-4} .

To quantify the AGN contribution at different luminosities, we identified either all or none of the continuum of each source as AGN according to the two scenarios described previously. We then determined the ratio $F_{5-10\mu\text{m}}(\text{Starformation})/F_{5-10\mu\text{m}}(\text{Total})$, with $F_{5-10\mu\text{m}}(\text{starformation})$ being the sum of UIB-dominated starburst flux and that part of the continuum flux that is ascribed to star formation under the given scenario. For each scenario, we averaged the results for the ULIRGs in each of the two luminosity bins. Table 5 displays the resulting average values along with their uncertainties. The average contribution of star formation to the 5-10 μ m flux is 65 to 84% for the

low luminosity bin and 24 to 33% for the high luminosity bin, the ranges representing the two extreme scenarios. Extrapolating from mid-infrared fluxes to total far-infrared ones, the average contributions of star formation are 82 to 94% for the low luminosity bin and 44 to 55% for the high luminosity bin. These results from quantitative modeling considerably reinforce the conclusions from the earlier work based on the L/C ratio: Low luminosity ULIRGs are predominantly starburst powered, while AGN powering dominates above $\sim 10^{12.4}$ to $10^{12.5} L_{\odot}$.

6. Conclusions

We have presented ISOCAM-CVF low resolution mid-infrared spectroscopy of 16 ultraluminous infrared galaxies obtained within a program targeted at investigating the most luminous ULIRGs. The data are analyzed along with the complete ISO database of low resolution spectra of ULIRGs/HYLIRGs, totalling 76 sources. We use the presence of the mid-infrared ‘UIB’ aromatic bands as a diagnostic of starburst activity, finding starburst-dominated systems up to a luminosity of $L_{\text{IR}} = 10^{12.65} L_{\odot}$. Other spectra show a strong AGN continuum with weaker features of uncertain origin. We have found one highly obscured AGN.

The mid-infrared spectra can be modeled in terms of a superposition of a UIB-dominated starburst spectrum and a continuum, both potentially strongly obscured. This continuum contains both AGN and additional H II region contributions. The fits prefer a two zone model in which the extinction to starburst and continuum regions may differ. Results from these fits agree well with previous simpler diagnostics based on the line-to-continuum of the UIB features.

Low luminosity ULIRGs are mostly starburst dominated, but the AGN fraction increases with luminosity and most ULIRGs above $\sim 10^{12.4}$ to $10^{12.5} L_{\odot}$ appear AGN like. We have separated ULIRGs into two luminosity bins of $L_{\text{FIR}} = 10^{11.8-12.4} L_{\odot}$ and $L_{\text{FIR}} = 10^{12.4-13.0} L_{\odot}$. We find that the average contributions of star formation to the infrared luminosity are 82 to 94% for the low luminosity bin and 44 to 55% for the high luminosity bin.

We are grateful to Michael Rowan-Robinson for allowing us access to the QDOT ULIRGs prior to publication. The work of QDT is supported by Verbundforschung (50 OR 9913 7). DCH acknowledges support from NASA grant NAG5-3359 to US ISO Observers. DR acknowledges support of the EC TMR Network ”Infrared Surveys” (under contract number ERBFMRX-CT96-0068). YT is supported by the Ministry of Education, Science, Sports and Culture of Japan under grants 10044052, and 10304013. SWS and the ISO Spectrometer Data Center at MPE are supported by DLR (DARA) under grants 50 QI 8610 8 and 50 QI 9402 3.

A. Reduction scheme for CVF observations of faint point sources

Aiming for a good CAM-CVF spectrum including a reliable continuum, a main source of uncertainty is due to the Point Spread Function (PSF). Because the width of the PSF changes with the observed wavelength, it is crucial to determine the observed total flux for each wavelength separately. This is easily done for bright point sources because it is easy to sum the observed flux over a large box (typically 5 by 5 pixels) or to fit the PSF profile to the observed image. Since our sources are point-like at CAM spatial resolution, it is not necessary to consider the complex situation for extended sources. Even for point sources, however, the PSF correction is difficult if they are faint. Then, only a few pixels around the brightest one have a significant S/N (hereafter the brightest pixel will be called “central pixel”). In such a case, the S/N of the corrected spectrum obtained by summing over a box or fitting the PSF profile is usually very low.

A better S/N can be obtained just using the signal of the central pixel and applying a PSF correction factor that varies slowly with wavelength. The main difficulty in determining this factor is to obtain the position of the source within the central pixel. This could be done by fitting a model of the PSF to the observed images at each wavelength. But, because the S/N is quite low for the pixels around the central pixel, direct application of this method gives uncertain positions and a final spectrum where the S/N is low, comparable to the S/N obtained by summing over a box. In order to improve the S/N we adopted the following method :

In CIA, theoretical PSFs are available at every half micron of the ISOCAM-CVF wavelength range, residual variations over such ranges are small. We divided the observed wavelength range into sub-ranges of one micron centered around the wavelength of a theoretical PSF, and summed images corresponding to wavelengths in this range of one micron around the given wavelength (i.e. about 10 images). We then fitted a PSF profile to the resulting image (hereafter the summed image). This method improves the S/N, and the deduced position of the source in the central pixel is known with a better confidence level. We used this position and the PSF to derive the correction factor from flux in the ‘central’ pixel to total flux, which was applied for each image in the considered wavelength range.

Although this method gives a better position of the source, it is still necessary to compute the systematic error introduced by this correction. The formal way is to compute the S/N for each pixel of the summed image, and then to use an inverse Monte-Carlo method to compute the S/N of the spectrum. Another equivalent way which avoids a Monte-Carlo simulation is to consider the images used to obtain the summed image *as guesses of a Monte-Carlo simulation* . This is equivalent to a simulation with ten guesses because the S/N of the summed image is deduced from these images. We then used the positions of the source obtained for all these images to correct the flux of the summed image. From the scatter of these measurements, it is then possible to deduce the systematic error introduced by the fitting method of the PSF profile.

Table 1: Basic data of ULIRGs observed with ISOCAM-CVF

| IRAS Name ^a | RA(2000) | DEC(2000) | z | S_{12} Jy | S_{25} Jy | S_{60} Jy | S_{100} Jy | $\text{Log}(L_{\text{IR}})$ L_{\odot} |
|------------------------|------------|-----------|-------|----------------|----------------|----------------|-----------------|--|
| F00183-7111 | 0:20:35.3 | -70:55:22 | 0.327 | <0.06 | 0.13 | 1.20 | 1.19 | 12.77 |
| 00188-0856 | 0:21:26.6 | -8:39:22 | 0.129 | <0.12 | 0.37 | 2.59 | 3.40 | 12.31 |
| 00275-2859 | 0:30:04.4 | -28:42:23 | 0.279 | <0.08 | 0.17 | 0.69 | 0.73 | 12.46 |
| 00406-3127 | 0:43:03.2 | -31:10:50 | 0.342 | <0.06 | <0.09 | 0.72 | 0.99 | 12.64 |
| 02113-2937 | 2:13:33.0 | -29:23:35 | 0.194 | <0.08 | <0.12 | 0.94 | 1.88 | 12.29 |
| F02115+0226 | 2:14:10.3 | 2:40:00 | 0.400 | <0.11 | <0.16 | 0.32 | 0.64 | 12.48 |
| F02455-2220 | 2:47:51.3 | -22:07:38 | 0.296 | <0.08 | <0.10 | 0.82 | 1.27 | 12.57 |
| 03000-2729 | 3:02:11.5 | -27:07:24 | 0.221 | <0.07 | <0.11 | 0.92 | 2.04 | 12.41 |
| 03538-6432 | 3:54:25.3 | -64:23:39 | 0.310 | <0.06 | 0.06 | 0.99 | 1.30 | 12.65 |
| 03521+0028 | 3:54:42.4 | 0:37: 8 | 0.152 | <0.25 | 0.23 | 2.64 | 3.83 | 12.46 |
| 04384-4848 | 4:39:50.8 | -48:43:11 | 0.213 | <0.04 | 0.07 | 0.99 | 1.34 | 12.32 |
| 17463+5806 | 17:47:04.6 | 58:05:24 | 0.309 | <0.04 | <0.04 | 0.65 | 0.95 | 12.48 |
| 18030+0705 | 18:05:32.5 | 7:06: 9 | 0.146 | <0.25 | <0.25 | 0.84 | 4.40 | 12.18 |
| 22192-3211 | 22:22:09.6 | -31:56:34 | 0.231 | <0.12 | 0.19 | 0.89 | 1.42 | 12.43 |
| 23515-2917 | 23:54:06.7 | -29:00:58 | 0.336 | <0.08 | <0.14 | 0.65 | 1.06 | 12.60 |
| F23529-2919 | 23:55:33.3 | -21:03: 7 | 0.430 | <0.08 | <0.16 | 0.33 | 0.63 | 12.55 |

Positions have been computed from the ISOCAM observations, with an accuracy of $\sim 5''$.

^aA name starting with an 'F' refers to a FSC object name. The others names are taken from the PSC.

Table 2: Detection of UIB features in the ULIRG spectra

| Iras Name | 6.2 μm | 7.7 μm | 11.3 μm | L/C | Note |
|-------------|-------------|-------------|--------------|------|-----------------------|
| F00183-7111 | n | n | n | 0.88 | |
| 00188-0856 | n | y | y | 1.53 | |
| 00275-2859 | n | y | n | 0.58 | |
| 00406-3127 | - | - | - | - | Not acquired |
| 02113-2937 | n | y | y | 2.53 | |
| F02115+0226 | n | n | n | - | No detection |
| F02455-2220 | n | y | n | - | (see Sect. 2.2) |
| 03000-2729 | n | y | y | 1.74 | |
| 03538-6432 | y | y | n | 1.70 | |
| 03521+0028 | n | y | y | 3.23 | |
| 04384-4848 | y | y | n | 2.08 | |
| 17463+5806 | n | y | n | 1.85 | |
| 18030+0705 | y | y | y | 1.88 | Large position offset |
| 22192-3211 | n | y | n | 0.85 | |
| 23515-2917 | n | y | n | 1.36 | |
| F23529-2919 | n | n | n | 0.38 | |

y : feature is significantly present (detected at 3σ expect for F02455-2220)

n : feature is doubtful or undetected

- : undefined

Table 3: Description of models used to fit ULIRG spectra and quality of spectral fits

| Model | Type of model | Number of parameters | $\frac{\chi^2}{N_{\text{free}}}$ All ULIRGs | $\frac{\chi^2}{N_{\text{free}}}$ High S/N Ulirgs |
|-------|--|----------------------|--|---|
| 1 a | $(\alpha_1 F_{\text{Stb}} + \alpha_2 F_{\text{AGN}}) \exp(-\beta A_{\text{DL}})$ | 4 | 2.48 | 4.79 |
| 1 b | $(\alpha_1 F_{\text{Stb}} + \alpha_2 F_{\text{AGN}}) \exp(-\beta A_{\text{GC}})$ | 4 | 2.24 | 4.30 |
| 2 | $(\alpha_1 F_{\text{Stb}} + \alpha_2 F_{\text{AGN}}) \exp(-\beta_1 A_{\text{DL}} - \beta_2 A_{\text{GC}})$ | 5 | 2.23 | 4.31 |
| 3 a | $\alpha_1 F_{\text{Stb}} \exp(-\beta_1 A_{\text{DL}}) + \alpha_2 F_{\text{AGN}} \exp(-\beta_2 A_{\text{DL}})$ | 5 | 1.70 | 2.81 |
| 3 b | $\alpha_1 F_{\text{Stb}} \exp(-\beta_1 A_{\text{DL}}) + \alpha_2 F_{\text{AGN}} \exp(-\beta_2 A_{\text{GC}})$ | 5 | 1.54 | 2.52 |
| 3 c | $\alpha_1 F_{\text{Stb}} \exp(-\beta_1 A_{\text{GC}}) + \alpha_2 F_{\text{AGN}} \exp(-\beta_2 A_{\text{DL}})$ | 5 | 1.64 | 2.79 |
| 3 d | $\alpha_1 F_{\text{Stb}} \exp(-\beta_1 A_{\text{GC}}) + \alpha_2 F_{\text{AGN}} \exp(-\beta_2 A_{\text{GC}})$ | 5 | 1.72 | 3.05 |
| 4 | $\alpha_1 F_{\text{Stb}} \exp(-\beta_{1,1} A_{\text{DL}} - \beta_{1,2} A_{\text{GC}})$ $+ \alpha_2 F_{\text{AGN}} \exp(-\beta_{2,1} A_{\text{DL}} - \beta_{2,2} A_{\text{GC}})$ | 7 | 1.42 | 2.21 |

F_{Stb} represents the starburst template spectrum (M82), F_{AGN} the powerlaw continuum. A_{DL} and A_{GC} are the extinction laws of (Draine & Lee 1984) and of the Galactic center, respectively.

Comparison of fit quality (see text) for the various models for all ULIRGs and for a high quality subset.

Table 4. Model results for ISOCAM-CVF and ISOPHOT-S targets

| IRAS Name | Cont/Star ^b | L/C ^b | IRAS Name | Cont/Star ^b | L/C |
|-------------|------------------------|------------------|-------------|------------------------|------|
| 00153+5454 | 0.0 | 3.34 | 17028+5817 | 0.47 | 3.58 |
| F00183-7111 | 5.31 | 0.88 | 17068+4027 | 0.0 | 1.40 |
| 00188-0856 | 1.48 | 1.53 | 17179+5444 | 1.59 | 1.38 |
| 00199-7426 | 6.26 | 1.08 | 17208-0014 | 0.07 | 5.54 |
| 00275-2859 | 100. | 0.57 | 17463+5806 | 2.38 | 1.85 |
| 00397-1312 | 100. | 0.22 | 18030+0705 | 0.60 | 1.88 |
| 01003-2238 | 100. | 1.44 | 18443+7433 | 6.09 | 1.70 |
| 01166-0844 | 0.00 | 2.16 | 18470+3233 | 100. | 0.68 |
| 01199-2307 | 0.00 | 0.97 | 18531-4616 | 1.59 | 2.59 |
| 01298-0744 | 1.79 | 1.50 | 19254-7245 | 3.47 | 0.89 |
| 01355-1814 | 0.00 | 0.93 | 19420+4556 | 0.0 | 3.69 |
| 01388-4618 | 0.00 | 3.93 | 19458+0944 | 0.0 | 2.44 |
| 01494-1845 | 0.00 | 1.95 | 20049-7210 | 0.0 | 3.77 |
| 01569-2939 | 100. | 1.14 | 20100-4156 | 0.0 | 1.92 |
| 02113-2937 | 0.64 | 2.53 | 20446-6218 | 0.0 | 0.94 |
| 02364-4751 | 0.66 | 3.48 | 20551-4250 | 0.42 | 2.33 |
| 02411+0354 | 0.18 | 3.17 | 21396+3623 | 0.0 | 2.31 |
| 03000-2719 | 0.88 | 1.73 | 22055+3024 | 1.12 | 0.96 |
| 03158+4227 | 0.53 | 1.72 | 22192-3211 | 100. | 0.84 |
| 03521+0028 | 0.21 | 3.23 | 22491-1808 | 1.04 | 2.85 |
| 03538-6432 | 1.45 | 1.70 | 23060+0505 | 100. | 0.08 |
| 04063-3236 | 100. | 2.55 | 23128-5919 | 0.96 | 2.86 |
| 04103-2838 | 100. | 1.37 | 23129+2548 | 0.0 | 3.55 |
| 04114-5117 | 1.03 | 0.97 | 23230-6926 | 0.58 | 1.50 |
| 04384-4848 | 0.93 | 2.08 | 23253-5415 | 0.79 | 1.58 |
| 06009-7716 | 1.64 | 3.63 | 23327+2913 | 0.0 | 0.97 |
| 06035-7102 | 0.92 | 1.11 | 23365+3604 | 0.0 | 4.47 |
| 06206-6315 | 0.33 | 3.69 | 23389-6139 | 0.0 | 1.33 |
| 06301-7934 | 0.48 | 1.02 | 23515-2917 | 2.87 | 1.36 |
| 06361-6217 | 2.0 | 0.67 | F23529-2119 | 15.32 | 0.38 |
| 09104+4109 | 100. | 0.48 | Arp220 | 0.0 | 4.20 |
| 12112+0305 | 0.39 | 3.13 | Mrk1014 | 100. | 0.62 |

REFERENCES

- Abergel, A., et al. 1996, *A&A*, 315, L73
- Alexander, D.M., Efstathiou, A., Hough, J.H., Aitken, D.K, Lutz, D., Roche, P.F., & Sturm, E. 1999, *MNRAS*, 310, 78
- Aussel, H., Gerin, M., Boulanger, F., Désert, F.X., Casoli, F., Cutri, R.M., & Signore, M. 1998, *A&A*, 334,L73
- Barger, A.J., Cowie, L.L., Sanders, D.B., Fulton, E., Taniguchi, Y., Sato, Y., Kawara, K., & Okuda, H. 1998, *Nature*, 394, 248
- Biviano, A., & Sauvage, M. 1999, in preparation
- Cesarsky, C.J., et al. 1996, *A&A*, 315, L32
- Cesarsky, D., et al. 1996, *A&A*, 315, L309
- Charmandaris, V., Mirabel, I. F., Tran, D., Laurent, O., Cesarsky, C. J., Gallais, P., Sauvage, M., & Vigroux, L. 1997 in: *Proceedings of the XVII Rencontres de Moriond, “Extragalactic Astronomy in the Infrared”*, Eds. G.A. Mamon, Trinh Xuan Thuan, and J. Tran Thanh Van, p.283
- Clavel, J. , et al. 2000, *A&A*, 357,,839
- Clements, D.L., Sutherland, W.J., Saunders, W., Efstathiou, G.P., McMahon, R.G., Maddox, S., Lawrence, & A., Rowan-Robinson, M. 1996, *MNRAS*, 279, 459
- Comastri, A., Setti, G., Zamorani, G., & Hasinger, G. 1995, *A&A*, 296, 1
- Condon, J.J., Huang, Z.-P., Yin, Q.F., & Thuan, T.X. 1991, *ApJ*, 378, 65
- Coulais, A., Abergel, A. 1999, in: *The Universe seen by ISO*, eds. P.Cox & M.F.Kessler, ESA SP-427, (Noordwijk: ESA), p. 61
- Crawford, T., Marr, J., Partridge, B., & Strauss, M.A. 1996, *ApJ*, 460, 225
- de Grijp, M.H.K., Miley, G.K., Lub, J., & de Jong, T. 1985, *Nature*,314,240
- Draine, B., & Lee, H. 1984, *ApJ*, 285, 89
- Dudley, C.C., & Wynn-Williams, C.G..1997, *ApJ*, 488, 720
- Duley, W.W., & Williams, D.A. 1981, *MNRAS*, 196, 269
- Fisher, K.B., Huchra, J.P., Strauss, M.A., Davis, M., Yahil, A., & Schlegel D. 1995, *ApJS*, 100, 69
- Genzel, R., et al. 1998, *ApJ*, 498, 579

Table 4—Continued

| IRAS Name | Cont/Starb ^a | L/C ^b | IRAS Name | Cont/Starb | L/C |
|------------|-------------------------|------------------|-----------|------------|------|
| 14348-1447 | 0.0 | 3.55 | Mrk231 | 100. | 0.31 |
| 15250+3609 | 0.46 | 2.88 | Mrk273 | 1.24 | 1.90 |
| 15307+3252 | 100. | 0.27 | NGC6240 | 0.0 | 2.58 |
| 16474+3430 | 0.35 | 3.58 | UGC5101 | 0.33 | 2.12 |
| 16487+5447 | 0.52 | 2.19 | ... | ... | ... |

The table includes the ISOPHOT-S (Rigopoulou et al. 1999) and CAM-CVF (this paper) ULIRGs.

^aRatio of the integrated mid-infrared fluxes contained in the continuum contribution and in the starburst contribution $F_{5-10\mu m}(\text{Continuum})/F_{5-10\mu m}(\text{Starburst})$ (Cont/Starb, not dereddened) computed with the model 3a

^bPAH Line to Continuum ratio

Table 5: Starburst luminosity to total luminosity ratio

| Luminosity | $\frac{F_{5-10\mu m}(\text{Starformation})}{F_{5-10\mu m}(\text{Total})}$ | | $\frac{F_{3-1000\mu m}(\text{Starformation})}{F_{3-1000\mu m}(\text{Total})}$ | |
|--------------------------|---|-------------|---|-------------|
| | scenario A | scenario B | scenario A | scenario B |
| $L < 10^{12.4}L_{\odot}$ | 65 ± 4 | 84 ± 4 | 82 ± 10 | 94 ± 10 |
| $L > 10^{12.4}L_{\odot}$ | 24 ± 7 | 33 ± 10 | 44 ± 17 | 55 ± 23 |

Scenario A : continuum is attributed only to AGN ; Scenario B : faint continua (<50% of the total MIR emission) are attributed to a starburst (see Section 5). The uncertainties are uncertainties of the mean value in one luminosity bin. The means of the two luminosity bins of a single scenario differ at 5 sigma in the MIR.

- Genzel, R., & Cesarsky, C.J. 2000, ARA&A, in press (astro-ph/0002182)
- Haas, M., Chini, R., Stickel, M., Lemke, D., Klaas, U., & Kreysa, E. 1998, ApJ, 503, L109
- Heckman, T.M. 1994, in: Mass-transfer induced activity in galaxies, ed. I. Shlosman, (Cambridge: Cambridge University Press), p.234
- d’Hendecourt, L., et al. 1996, A&A, 315, L365
- Hines, D. C., Schmidt, G.D., Smith, P. S., Cutri, R. M., & Low, F. J. 1995, ApJ, 450, L1
- Hines, D. C., Schmidt, G. D., Wills, B. J., Smith, P. S., & Sowinski, L. G. 1999, ApJ, 512, 145
- Hughes, D.H., et al. 1998, Nature, 394, 241
- Kessler, M.F., et al. 1996, A&A, 315, L27
- Kim D.C. 1995, PhD Thesis, University of Hawaii
- Laurent, O., Mirabel, I.F., Charmandaris, V., Gallais, P., Vigroux, L., & Cesarsky C.J. 1999, in: The Universe as seen by ISO, eds. P. Cox and M.F. Kessler, ESA SP-427 (Noordwijk: ESA), p. 913
- Lawrence, A., et al. 1999, MNRAS, 308, 897
- Léger, A., & Puget, J.-L. 1984, A&A, 137, L5
- Lutz, D., et al. 1996 A&A, 315, L269
- Lutz, D., Spoon, H.W.W., Rigopoulou, D., Moorwood, A.F.M., & Genzel, R. 1998, ApJ, 505, L103
- Lutz, D., Veilleux, S., & Genzel, R. 1999, ApJ, 517, L13
- Lutz, D. 1999, in: The Universe as seen by ISO, eds. P. Cox and M.F. Kessler, ESA SP-427 (Noordwijk: ESA), p. 623
- Lutz, D., Sturm, E., Moorwood, A.F.M., Alexander, T., Netzer, H., & Sternberg, A. 2000 ApJ, 536, 697
- Meurer, G.R., Heckman, T.M., Lehnert, M.D., Leitherer, C., & Lowenthal, J. 1997, AJ114, 54
- Mirabel, I.F., et al. 1998, A&A, 341, 667
- Mirabel, I.F., et al. 1998, A&A, 333, L1
- Moorwood, A.F.M. 1986, A&A, 166, 4
- Moorwood, A.F.M. 1999, in: The Universe as seen by ISO, eds. P. Cox and M.F. Kessler, ESA SP-427 (Noordwijk: ESA), p. 825

- Papoular, R., Conrad, J., Giuliano, M., Kister, J., & Mille, G. 1989, *Å*, 217, 204
- Pier, E.A., & Krolik, J.H. 1992, *ApJ*, 401, 99
- Rigopoulou, D., Spoon, H.W.W., Genzel, R., Lutz, D., Moorwood, A.F.M., & Tran, Q.D 1999, *AJ*, 118, 2625
- Roche, P.F., Aitken, D.K., Smith, C.H., & Ward, M.J. 1991, *MNRAS*, 248, 606
- Roussel, H., Sauvage, M. & Vigroux, L. 2000, in preparation
- Roelfsema, P.R., et al. 1996, *A&A*, 315, L289
- Sakata, A., Wada, S., Onaka, T., & Tokunaga, A.T. 1987, *ApJ*, 320, L63
- Sanders, D.B., Soifer, B.T., Elias, J.H., Madore, B.F., Matthews, K., Neugebauer, G., & Scoville, N.Z. 1988, *ApJ*, 325, 74
- Sanders, D.B., Soifer, B.T., Elias, J.H., Neugebauer, G., & Matthews, K. 1988a, *ApJ*, 328, L35
- Sanders, D.B., & Mirabel, I.F. 1996, *ARA&A*, 34, 725
- Solomon, P.M., Downes, D., Radford, S.J.E. & Barrett, J.W. 1997, *ApJ*, 478, 144
- Soifer, B.T., Neugebauer, G., Matthews, K., Egami, E., Becklin, E.E, Ressler, M., Werner, M.W., Weinberger, A.J, Evans, A.S., Scoville, N., Surace, J.A., & Condon, J.J. 2000, *ApJ*, 119, 509
- Schutte, W. 1998 in *Solid Interstellar Matter : the ISO revolution (Les Houches Workshop, February 2-6)*, EDP Sciences.
- Starck, J.L., Abergel, A. & Aussel, H. 1999, *A&AS*, 134, 135
- Sturm, E., et al. 1996, *A&A*, 315, L144
- Sturm, E., Lutz, D., Tran, D., Feuchtgruber, H., Genzel, R., Kunze, D., Moorwood, A.F.M., & Thornley, M. 2000, *A&A*, 358, 481
- Taniguchi, Y., Sato, Y., Kawara, K., Murayama, T., & Mouri, H. 1997, *A&A*, 318, L1
- Taniguchi, Y., Yoshino, A., Ohyama, Y., & Nishiura, S. 1999, *ApJ*, 514, 660
- Tran, D. 1998, PhD thesis, Université de Paris XI
- Verstraete, L., Puget, J.-L., Falgarone, E., Drapatz, S., Wright, C.M., & Timmermann, R. 1996, *A&A*, 315, L337
- Veilleux, S., Sanders, D. B. & Kim, D.C., 1999, *ApJ*, 522, 139
- Vigroux L., et al. 1996, *A&A*, 315, L93

Vigroux L., et al. 1999, in: The Universe as seen by ISO, eds. P. Cox and M.F. Kessler, ESA SP-427 (Noordwijk: ESA), p. 805

Fig. 1.— Histogram of infrared luminosities for ULIRGs with low resolution ISO mid-infrared spectroscopy (taken from ISOPHOT-S observations (Rigopoulou et al. 1999) and ISOCAM-CVF observations (this paper)). Sources with ISOCAM-CVF spectra shown in this paper are shaded. The combined sample shown here is biased towards high luminosity ULIRGs.

Fig. 2.— Mid-infrared spectra of sources observed with ISOCAM. Shaded regions represent the sum of RMS and systematic error, as described in section 2.2. Positions of the 6.2, 7.7, 8.6 and 11.3 μm features are indicated in each plot. We also plot the uncorrected spectrum of IRAS F02455-2220 which should be considered a lower limit (see text). An upper limit is given for IRAS 02115+0226. Wavelengths are rest-frame wavelengths.

Fig. 3.— Comparison between the L/C diagnostic of the 7.7 μm band adopted by Genzel et al. (1998) and subsequent papers, and a narrow band diagnostic using just the ratio of fluxes at 7.7 and 6 μm for Galaxies observed by PHOT-S (Rigopoulou et al. 1999), SWS (Sturm et al. 2000), and CAM-CVF (this paper). Upper and lower limits have been suppressed in this plot. The overplotted line shows the expected relation if the underlying continuum is flat.

Fig. 4.— Comparison of the extinction laws described in section 4. The Draine and Lee law is lower than the Galactic center law. The squares represent the extinction law towards the GC derived from hydrogen lines (Lutz 1999a).

Fig. 5.— Examples of model fits to ULIRG spectra, using model 3a. The figure includes high and low S/N spectra, and AGN-dominated and starburst-dominated spectra to show the success of the fitting procedure in all those cases. Data are shown by thin lines while the fitted spectra are shown by thick lines.

Fig. 6.— Test of the quality of the two model classes, using mixed starburst/AGN templates (upper plots: Cen A, lower plots: Circinus). The left plots show models (3a) where starburst and AGN are subject to different levels of extinction, while the extinction is identical for both components in the right plots (model 2). Models with different extinction for AGN and starburst are clearly favored.

Fig. 7.— Comparison of the fitted spectrum and the model (3a) with the starburst templates M83, NGC3256, NGC 6946 and NGC 253. The thin plain line is the observed spectrum, the thick line is the model spectrum, the dashed line is the continuum contribution and the dotted line is the starburst contribution.

Fig. 8.— Comparison of the fitted spectrum and the model for the continuum/AGN templates spectrum : SgrA* (model 3b) and NGC 1275, NGC 1068 and NGC 5506 (model 3a). The thin plain line is the observed spectrum, the thick line is the computed spectrum, the dashed line is the continuum contribution and the dotted line is the starburst contribution (not visible for GC-SgrA and NGC 1275). The GC SgrA spectrum is not perfectly reproduced at short wavelengths because of the extinction law used.

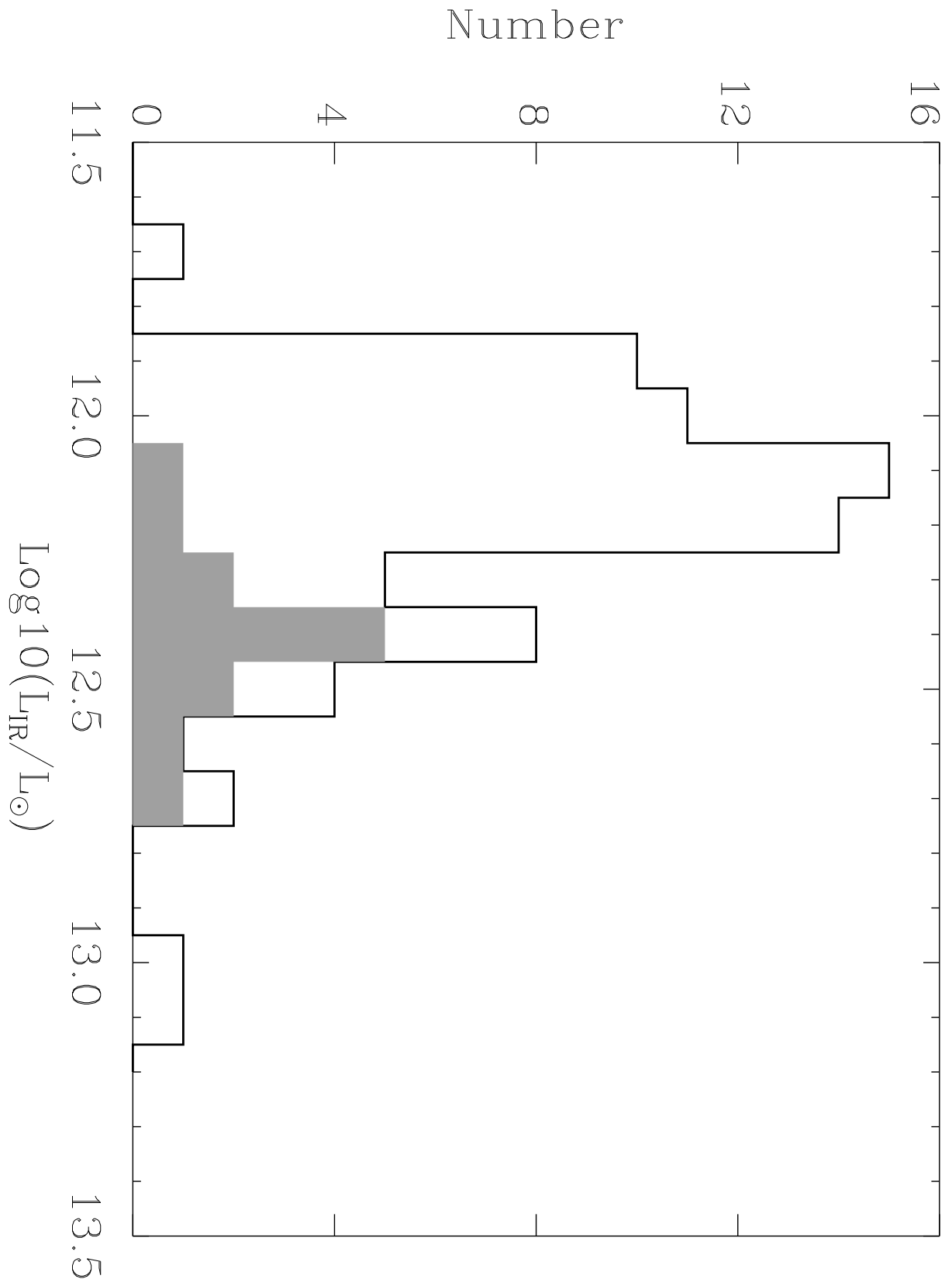
Fig. 9.— Comparison of the fitted spectrum and the model for the mixed templates : Circinus (observed by SWS, (Sturm et al. 2000)), Centaurus A, Mrk 273 and NGC 7469. Graphical conventions are the same than in Figure 8. The observed AGN spectra of CenA (Mirabel *et al.* 1999), and Circinus (Moorwood et al. 2000), observed with ISOCAM-CVF, are overplotted (thick plain line) and compared to the continuum component deduced from the model. In both cases, the observed AGN component is similar to the continuum contribution derived from the model.

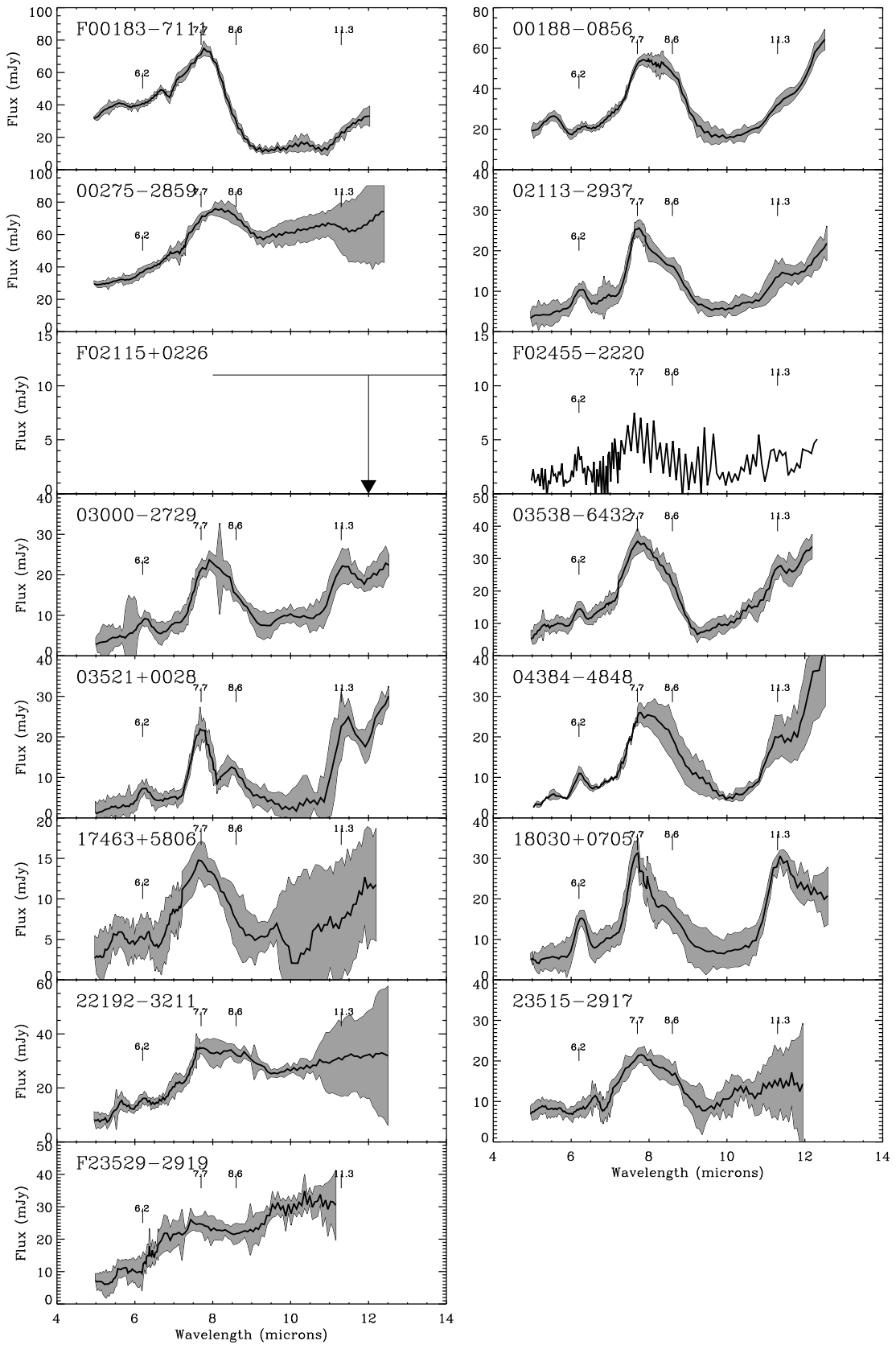
Fig. 10.— Comparison between the L/C ratio of the 7.7 μm band and the ratio of 5-10 μm Continuum and starburst UIB spectrum ($F_{5-10\mu\text{m}}(\text{Continuum})/F_{5-10\mu\text{m}}(\text{Starburst})$) given by the fit 3a (not dereddened). Squares represents ULIRG points, diamonds starbursts, and triangle AGNs. A 5-10 μm continuum to starburst flux ratio greater than 50 is representative of a spectrum dominated by the continuum component. In order to maintain readability of the figure we assigned to those galaxies arbitrary continuum to band flux ratio near 100.

Fig. 11.— Line to continuum ratio of the 7.7 μm feature as a function of the IR luminosity. The little asterix and upper limits are from the sample of ULIRG observed by PHOT-S (Lutz et al. 1998; Rigopoulou et al. 1999). Observations of hyperluminous galaxies (Taniguchi et al. 1997; Aussel et al. 1998) are added.

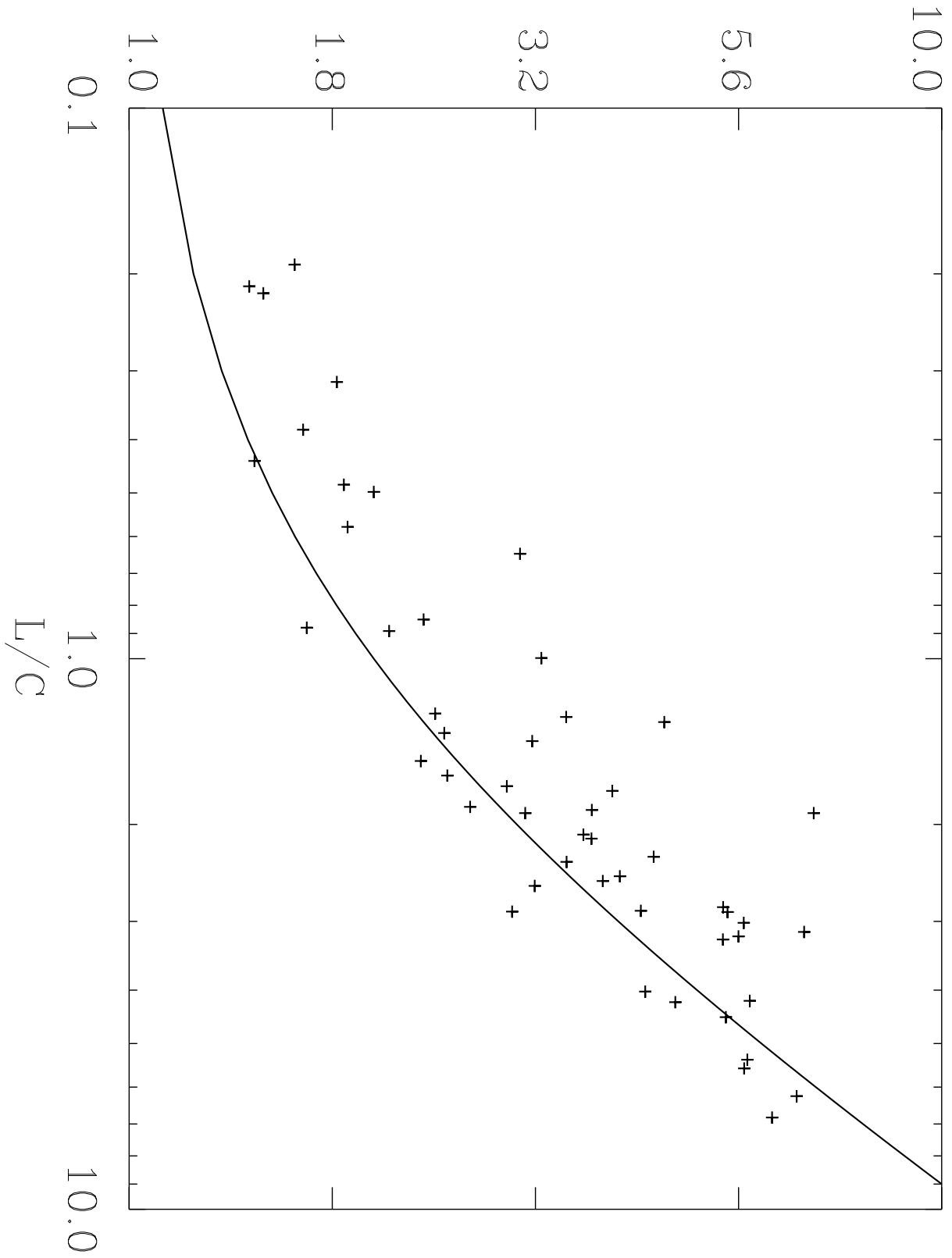
Fig. 12.— Comparison of the spectra of Arp220 and the strong star forming region in the overlap region of NGC4038/4039 (KnotA , Vigroux et. al (1996), Mirabel et al. (1998)). The graphical convention are as described for Figure 8.

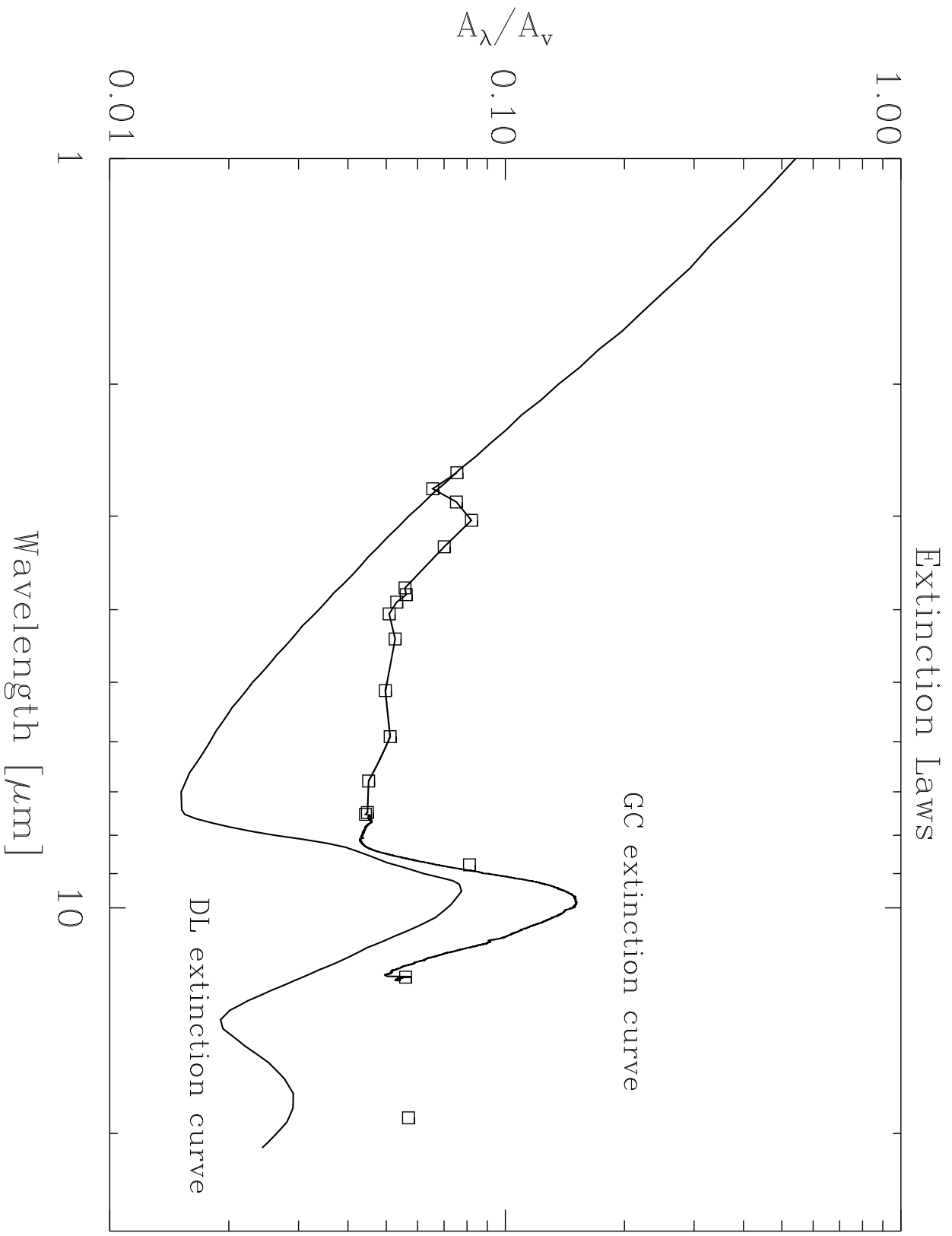
Fig. 13.— Trend of the mid-infrared ratio $F_{5-10\mu\text{m}}(\text{Starburst})/F_{5-10\mu\text{m}}(\text{Total})$ (not dereddened) versus infrared luminosity. At each luminosity, the plot shows the median $F_{5-10\mu\text{m}}(\text{Starburst})/F_{5-10\mu\text{m}}(\text{Total})$ of the 17 galaxies from Table 4 and (Taniguchi et al. 1997; Aussel et al. 1998) closest to the considered luminosity. The right axis displays the extrapolated bolometric ratio $F_{3-1000\mu\text{m}}(\text{Starformation})/F_{3-1000\mu\text{m}}(\text{Total})$ as described in section 4.3.

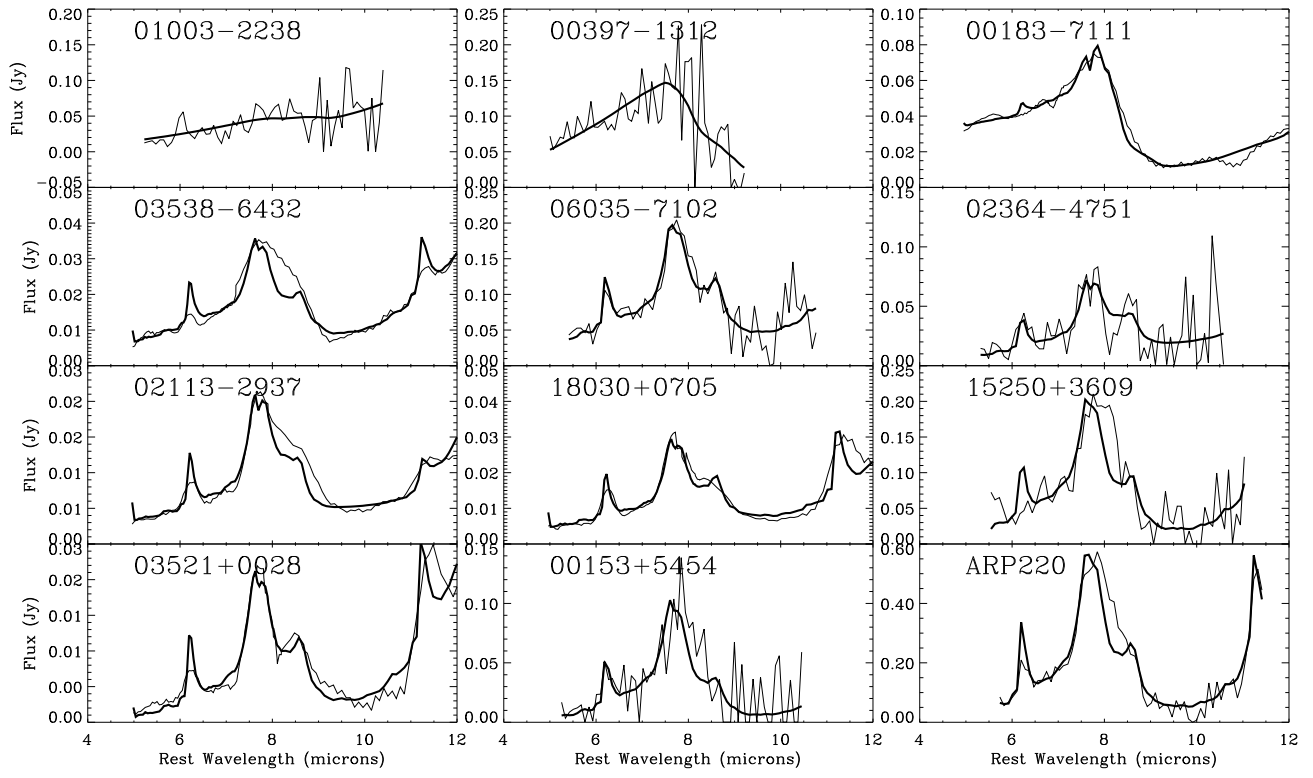


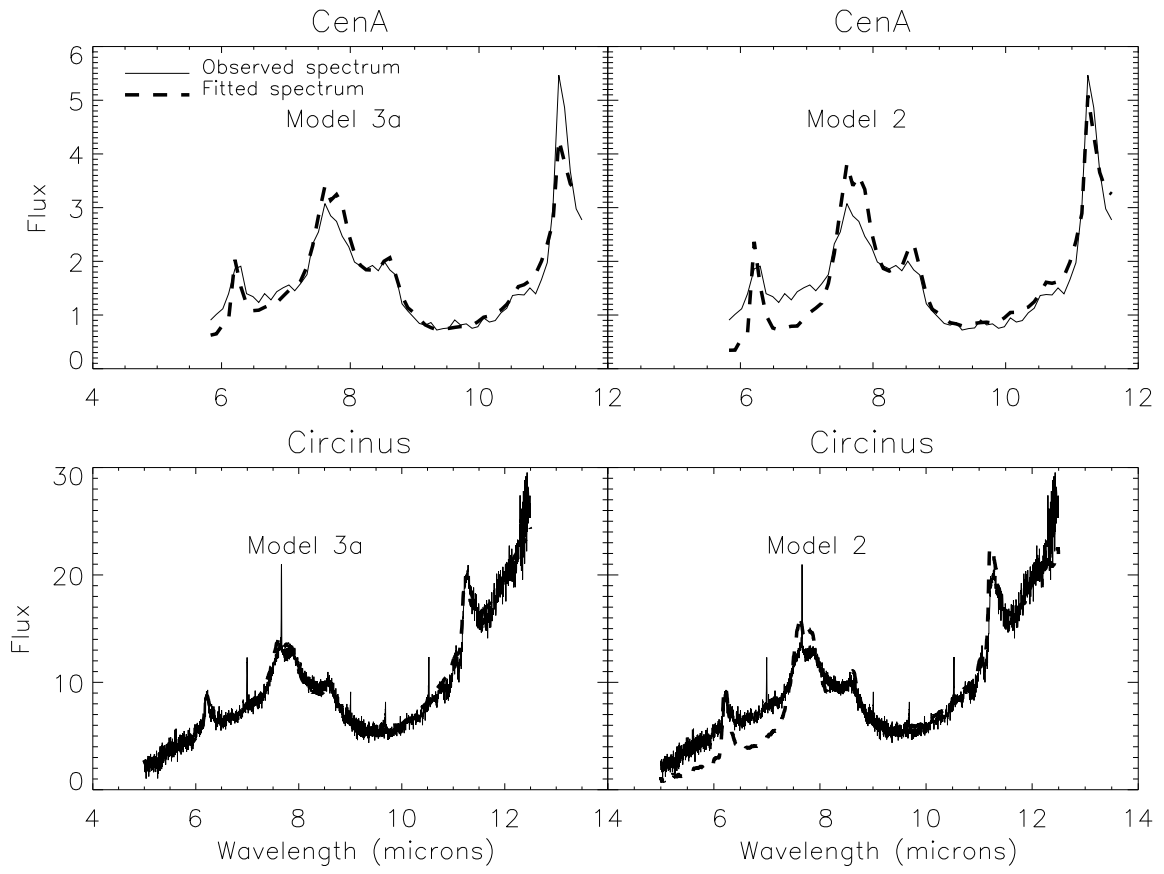


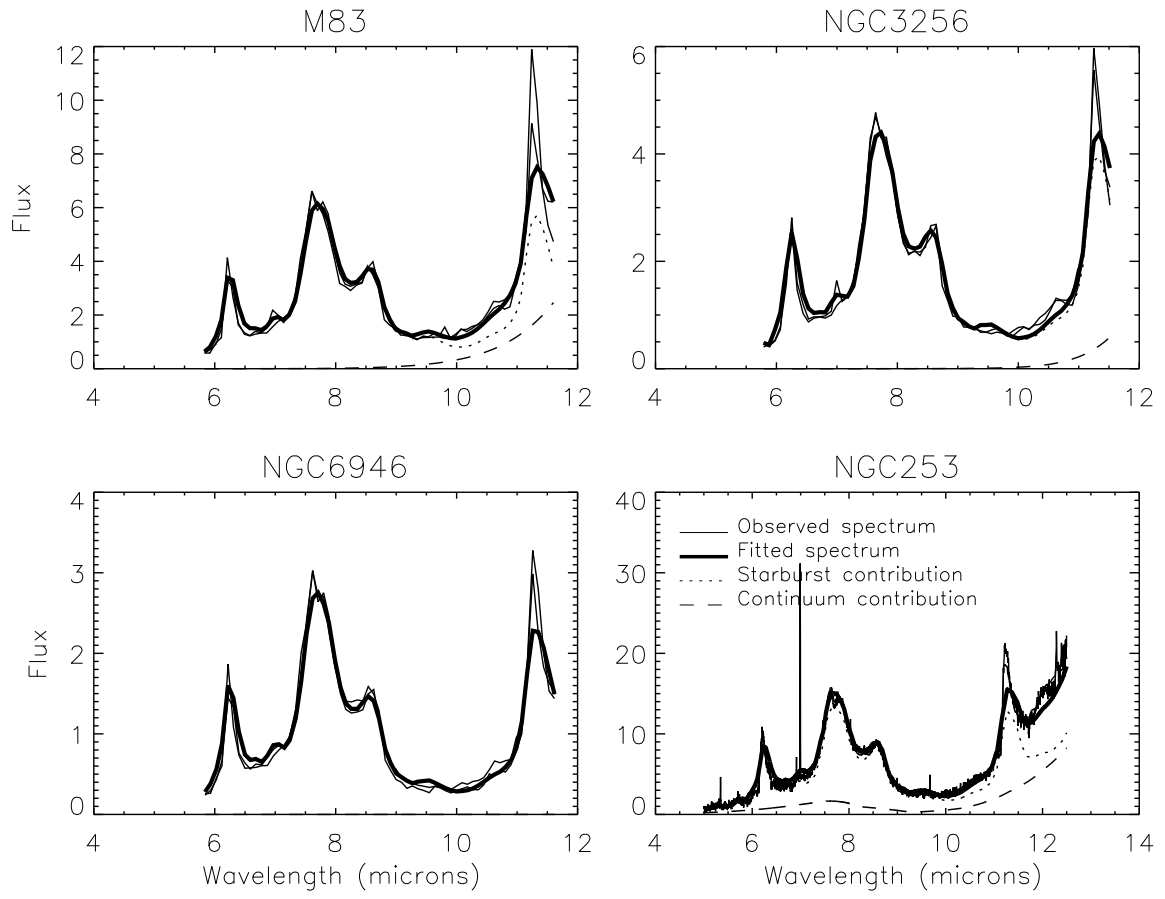
$F(7.7)/F(6.0)$

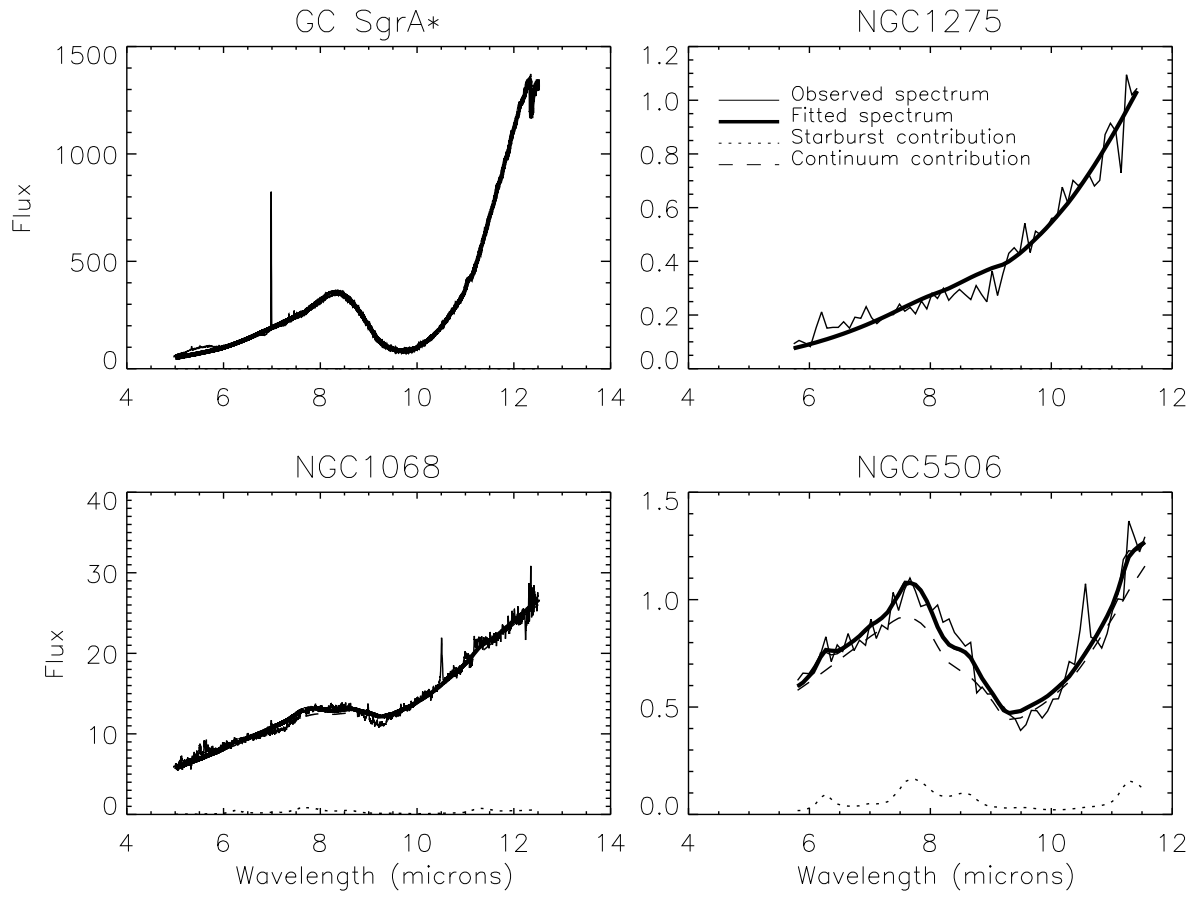


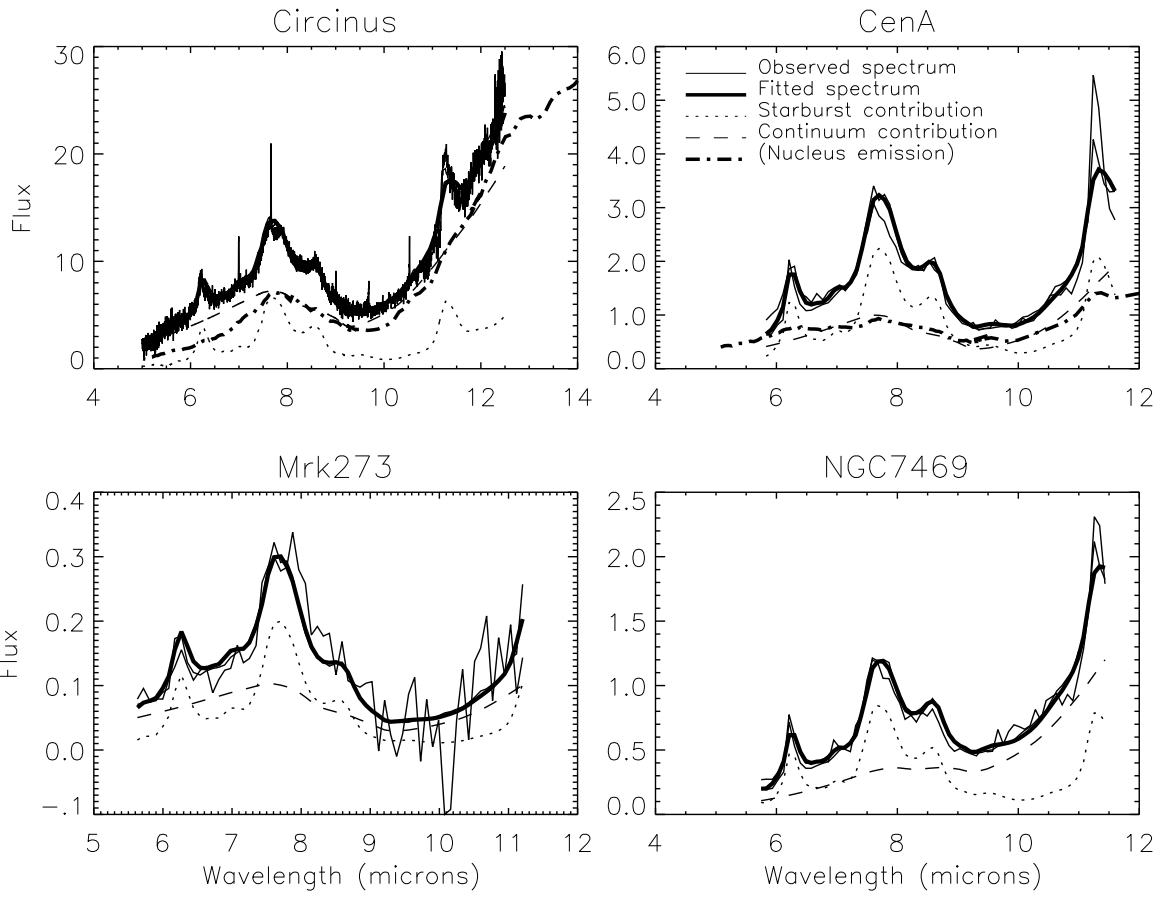




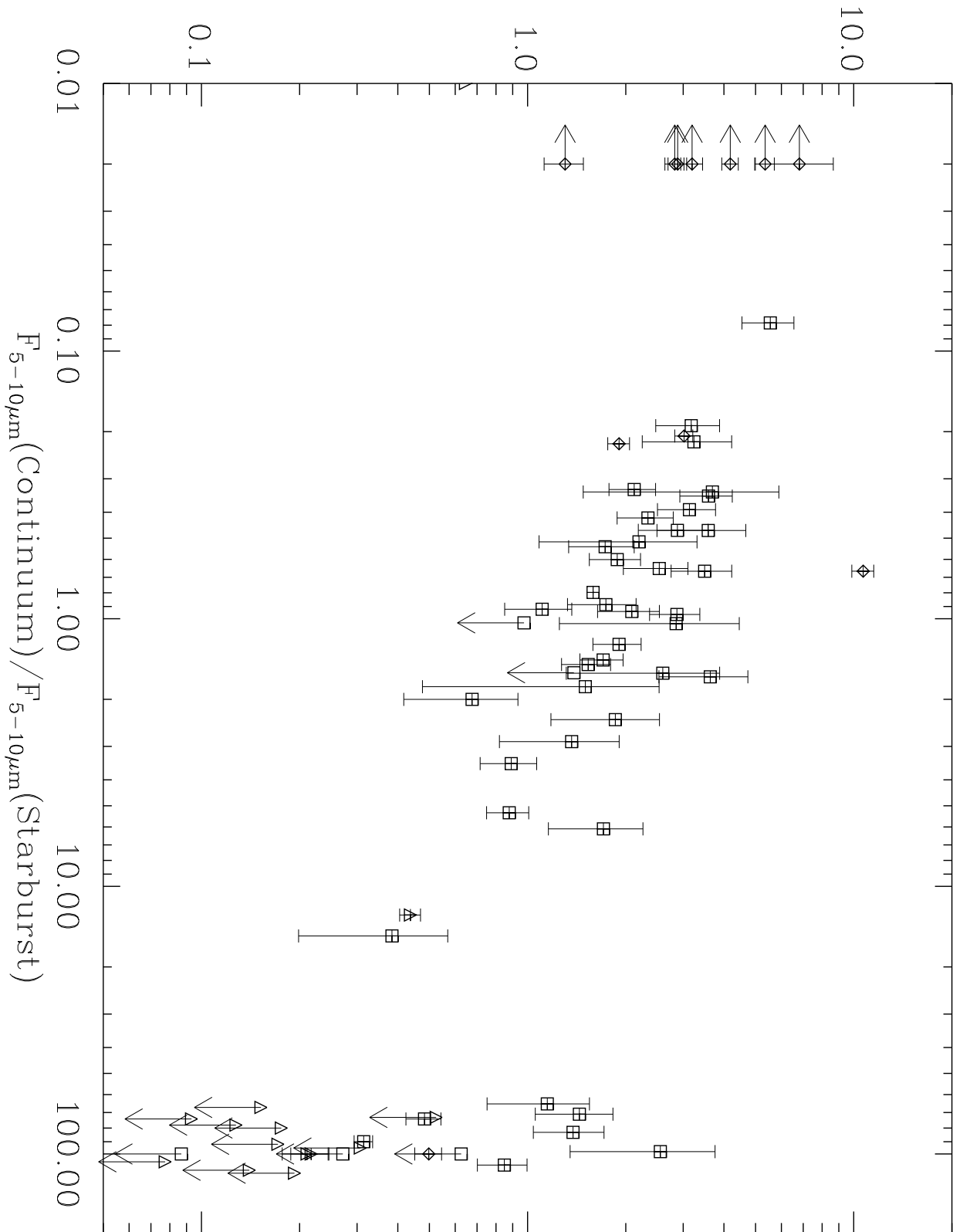


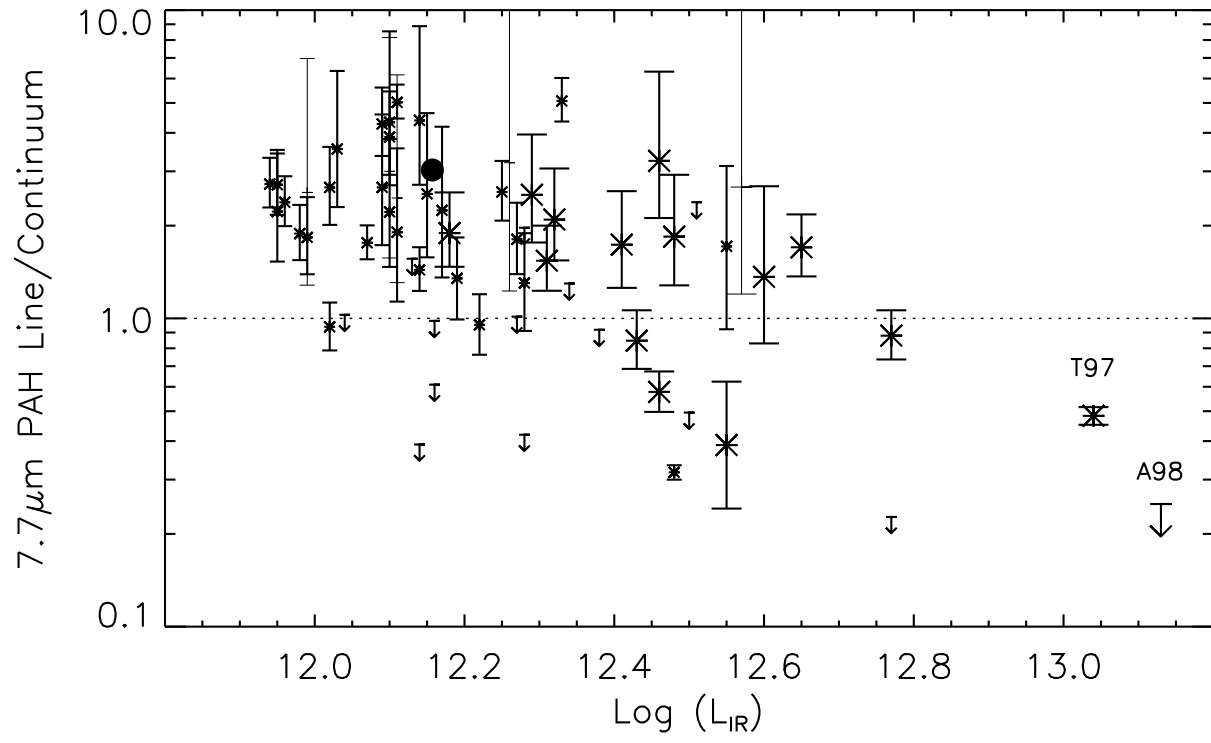




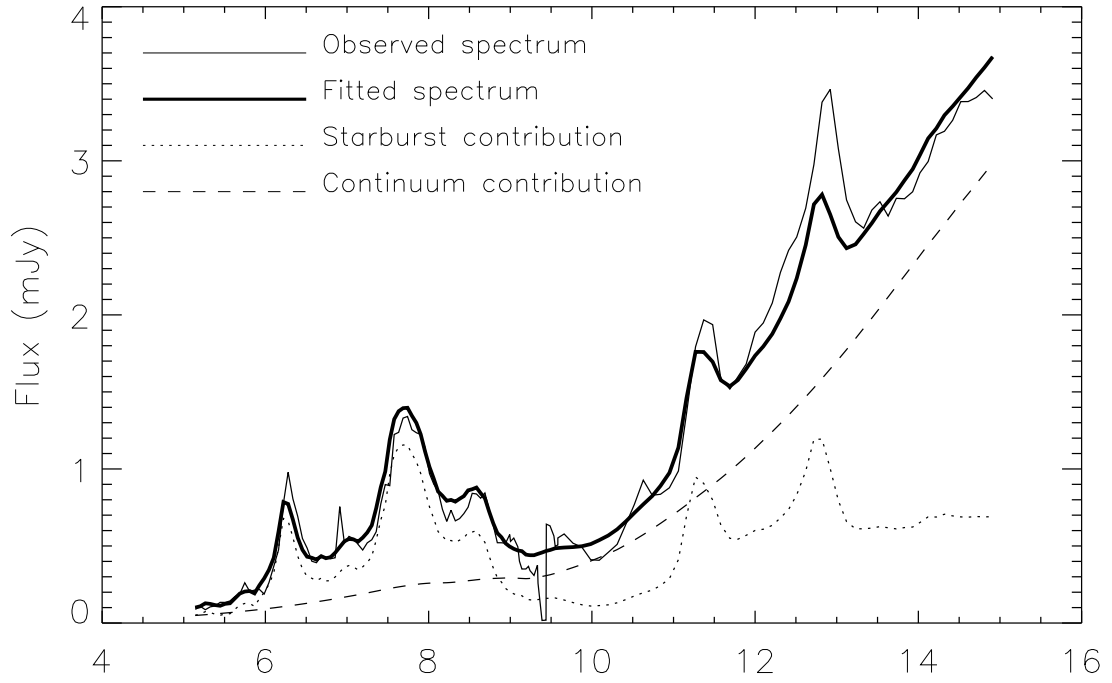


L/C (7.7 microns)





NGC4038/39- Knot A



Arp 220

